Contract DAAL01-96-2009
Final Report
August 5, 1996

Microwave Radiometer for Passively and Remotely Measuring Atmospheric Temperature, Water Vapor, and Cloud Liquid Water Profiles

Dr. Fredrick Solheim, PI
John R. Godwin, Science Team
Dr. Randolph Ware, Science Team
2898 30th Street
Boulder, CO 80301-1212
(303) 449-9192
fax: (303) 786-9343

Submitted to:
Army Research Laboratory
AMSRL BE W
Attn: Dr. Ed Measure
Battlefield Environment Directorate
WSMR NM 88002-5501

with a copy to:
DTIC
ATTN: Document Acquisition
Cameron Station
Alexandria, VA 22304-6145

SBIR Program License Rights to Technical Data

License Rights Legend

Contract DAAL01-96-2009
Contractor: Radiometrics Corporation

For a period of two (2) years after the delivery and acceptance of the last deliverable item under this contract, this technical data shall not, without the written permission of the above Contractor, be either (a) used, released or disclosed in whole or part outside the Government, (b) used in whole or in part by the Government for manufacture, or (c) used by a party other than the Government. After the expiration of the two year period, the Government amy use, duplicate, or disclose the data, in whole or in part and in any manner, for Government purposes only, and may or permit others to do so for Government purposes only. All rights to use or duplicate this data in whole or in part for commercial purposes are retained by the Contractor, and others to whom this data may be disclosed agree to abide by this commercial purposes limitation. The Government assumes no liability for use or disclosure of the data by others for commercial purposes. This legend shall be included on any reproduction of this data, in whole or part.

Nothing contained in this clause shall imply a license to the Government under any patent or be construed as affecting the scope of any license or other right otherwise granted to the Government under any patent.

Certification of Technical Data Conformity

The contractor, Radiometrics Corporation, hereby certifies that, to the best of its knowledge and belief, the technical data delivered herewith under Contract DAAL01-96-2009 is complete, accurate, and complies with all the requirements of the contract.

___________________________________ date _______________
Fredrick Solheim, Principal Investigator

Table of Contents

List of Figures

List of Tables

1. Introduction

(1.a) Motivation for radiometric atmospheric profiling

In spite of their inaccuracies, cost, sparse temporal sampling, and logistical difficulties, radiosondes (RAOBs) are still the fundamental method for atmospheric temperature, wind, and water vapor profiling. A better technology has been pursued for decades, but until now, no accurate continuous all-weather technology has been demonstrated. The highly stable frequency agile Radiometrics radiometer temperature and water vapor profilers (the subject of this study) rival the accuracy of RAOBs, while giving continuous profiles. We also have the capability to profile cloud liquid water, a capability absent in RAOBs. There are no other sensor systems that can profile cloud liquid.

Applications for this passive profiling capability include weather forecasting and nowcasting, detection of aircraft icing and other aviation related meteorological conditions, determination of density profiles for artillery trajectory and sound propagation determinations, refractivity profiles for radio ducting prediction, corrections to VLBI and GPS measurements, atmospheric radiation flux studies, and measurement of water vapor densities as they affect hygroscopic aerosols and smokes.

This report details our Phase I efforts and the findings. For the reader/reviewer with limited time, the most salient findings and conclusions regarding the performance and design of the profiling instrument are contained in this introductory **Chapter 1, Chapter 4** (comparison of performance of the retrieval methods), **Chapter 5** (hardware design of the profiling radiometer), **Chapter 6** (conclusions), and **Appendix B** (sample retrieved profiles).

(1.b) Microwave Profiling Methodology - Background

(1.b.1) Profiling of Temperature

Radiometric temperature profiling can be accomplished by measuring the brightness spectrum at points along the side of the oxygen feature at 60 GHz (Westwater, 1965). By scanning outward from line center, where the opacity is so great that all signal originates from just above the antenna, onto the wing of the line, where the radiometer “sees” deeper (higher) into the atmosphere, altitude information is obtained. Emission at any altitude is proportional to local temperature; thus the temperature profile can be retrieved. Either shoulder of this feature is suitable for retrieval of temperature profile information.

(1.b.2) Profiling of Water Vapor

Information on the vertical distribution of water vapor is contained in the intensity and shape of the emission from pressure broadened water vapor lines. At high altitude, the emission from water vapor is in a narrow line, and at low altitudes this line is pressure broadened. The intensity of emission is proportional to vapor density. Scanning the emission profile and mathematically inverting the observed data can therefore yield water vapor profiles.

The water vapor line at 183 GHz is used for vapor profiling from satellites. The high opacity of this line hides the unknown emission emenating from the earth’s surface, eliminating this error soruce but precluding profiling to low altitudes. The line at 22 Ghz is too transparent for effective profiling from satellites but is suitable for ground-based profiling.

Because of the spatial and temporal variability of water vapor, it is implied that the same sample of sky must be observed for all spectral frequencies for water vapor profiling. This would require that only one elevation angle be utilized, and that all frequencies be simultaneously observed. However, observing at a multitude of frequencies simultaneously is not practical. Also, there is additional information to be gained by observing at several elevation angles. Further, just as a RAOB is a line trajectory sample, a radiometric observation along a single path is not representative of the water vapor distribution. Averaging with numerous observation cycles and at several elevation angles may therefore be justified. Kalman filtering techniques may be effective in improving retrieved profiles.

(1.b.3) Profiling of Cloud Liquid

While profiling of water vapor and temperature are accomplished utilizing resonances, cloud liquid has no spectral features, but instead contributes to the brightness temperature in the microwave region as *(frequency)*^{2}. To obtain altitude information, profiling of cloud liquid must therefore be accomplished by measuring its contribution to known (or measured) atmospheric spectral features whose opacity varies with frequency. For instance, as described above, the atmospheric temperature profile can be obtained by scanning either side of the 60 GHz oxygen feature. Scanning from line center outward onto either of the wings of the feature moves the observation deeper and deeper into the atmosphere, yielding altitude information on atmospheric temperature. Cloud liquid water, if present, contributes more to the high frequency side (60 to 75 GHz) of this feature than to the low frequency side (45 to 60 GHz) and skews the line shape. Therefore, scanning *both* sides of the line yields information on the temperature *and* cloud liquid profiles. There is also liquid profile information in the 22 to 29 GHz + 52 to 59 GHz tuning bands, as will be shown herein.

(1.c) The Radiometrics microwave radiometer design

Radiometrics Corporation has developed an advanced passive microwave radiometer design based on a highly stable tunable synthesized local oscillator in the receiver. This design overcomes errors induced by receiver frequency drift in other current generation designs, while allowing observation of a large number of frequencies across wide tuning ranges. The number of eigenvalues in the radiometer observations, and therefore the information content, is thereby maximized. The result is more accurate and resolute atmospheric temperature, pressure, water vapor, and cloud liquid profiles. U.S. patent on the synthesized design and on a highly accurate cryogenic calibration target has been issued, and Canadian and European patents are pending. A previously issued Radiometrics patent covers our gain-stable receiver design.

Various local oscillators (YIG, DRO, varactor tuned Gunn, and others) have been proposed by others for tunable radiometers and have been previously investigated by Radiometrics. All suffer from frequency drift and uncertainty in the frequency output which result in error in the retrieved atmospheric profile. A 10 MHz oscillator drift in a 60 GHz temperature profiler, for instance, results in a 1C error in the retrieved profile. YIG oscillator designs can drift as much as 30 MHz (3C profile error). Phase lock looping tunable oscillators can bring stability down to several Hz, while coincidentally bringing the design into the realm of our synthesized receiver patent coverage. YIGs and Gunns are power consumptive and therefore dissipate significant heat.

Digital signal processing (DSP) methods have been investigated and rejected by Radiometrics because of the limited sampling bandwidth and high cost of DSP at high frequencies (wide bandwidths), while offering no advantage over other methods. Additionally, block down conversion is required to bring the receiver information into the frequency range of current DSP technology; this requires a highly stable (synthesized) local oscillator. So DSP methods require additional high cost hardware over Radiometrics' design, while limiting performance.

Our radiometer is a total power receiver with a highly stable noise diode as a gain reference. The resolving power (called delta T) of this design is superior to autocorrelation, Dicke, balanced Dicke, and noise adding receivers. This design has evolved over more than 10 years, and has resulted in a highly accurate and capable, yet economical, profiling radiometer design.

(1.d) The Army ASL Phase I development effort reported herein

In this Phase I effort, Radiometrics has applied our above design to a water vapor profiling radiometer concept. This design effort included identifying vendor sources for critical items such as the antenna isolator to span the tuning range, the tunable synthesizer, the frequency quadrupler, and the broadband biased mixer. The performance of the radiometer, based on the performance of each of the individual receiver components, was theoretically determined.

Based on the expected performance of a synthesized total power radiometer, we have performed eigenvalue analysis to determine the optimum frequency tuning range, and frequency/elevation angle ensemble within said tuning range. We expanded the eigenvalue analysis beyond the original scope of the proposal by determining the optimum frequency ensemble for the existing White Sands/Radiometrics microwave temperature profiler (MTP). The major part of the Phase I effort was to investigate mathematical inversion methods to convert the radiometer observables (the power spectrum measured by the radiometer) into water vapor profiles. We simulated retrieval of 3 years of temperature, water vapor, and cloud liquid profiles based on RAOBs from Denver, Oklahoma City, and West Palm Beach. Four promising mathematical inversion methods were applied: the Newton's method retrieval of Han/Westwater, neural networking, direct inversion of the VanVleck pressure broadening model, and Bayesian maximum probability methods. The direct inversion of the VanVleck model requires no *a priori* statistical knowledge. Standard statistical retrievals were also accomplished for use as a benchmark. Results of this intercomparison is included herein.

We also investigated the application of monolithic microwave integrated circuit (MMIC) technology to radiometers. MMIC technology is now being commercially produced for the telecommunications industry; conversion of commercially available receivers may be possible and would reduce the size and cost of radiometers while increasing robustness.

We have, through this Phase I effort, demonstrated the feasibility of constructing a water vapor profiling radiometer based on our current total integrated water vapor and temperature profiling radiometer design. The modeling that we performed in Phase I demonstrated an impressive ability to retrieve water vapor profiles in all weather conditions. We further determined the ability of a hypothetical combined MTP/water vapor profiler, having the ability to tune across wavebands in the 20 to 30 GHz and in the 45 to 60 and 60 to 75 GHz ranges, to retrieve ***profiles of cloud liquid***.

(1.e) Personnel performing this contract

The personnel performing this contract are Dr. Fredrick Solheim, PI, John R. Godwin, Science Team, and Dr. Randolph Ware, Science Team. Consultants are Dr. Ed Westwater and Dr. Yong Han of NOAA ETL and Steve Keihm and Dr. Ken Marsh of JPL.

2. Selection and eigenvalue analysis of the observables of the proposed radiometer

(2.a) Determination of receiver tuning bandwidth hardware capability

We have determined that we can build a K band receiver that will tune across 7.2 GHz. Critical to this capability are: availability of a synthesizer that can span the required frequencies, an antenna isolator that will perform across 20 to 29 GHz and at 31.4 GHz, and a biased mixer that is also capable across this range. We have identified a mixer, antenna isolator, and antenna feed horn that will operate adequately across this waveband. The receiver noise figure is estimated to be no more than 0.7 dB higher than our existing 23.8 and 31.4 GHz dual channel receiver (about 5 dB).

We calculated eigenvalues for two placements of this K band tuning capability and found that 22 to 29 GHz is equal to or superior to 20 to 27 GHz in information content for the three atmospheric parameters to be profiled.

We have also determined that we can build a V band receiver that will tune across at least 6 GHz or 9 GHz, depending upon whether we quadruple the LO drive or double and then triple (2x3=6). We have identified a mixer and antenna isolator that will operate over 50 to 60 GHz. Eigenvalue analysis tells us that, for profiling of cloud liquid, a frequency below the V band (50 to 75 GHz) is desirable. Although 48 GHz is below the recommended operating frequency of WR15 waveguide, it is still above the cutoff frequency of 39.4 GHz for this waveguide and therefore might be utilized at slightly higher losses (negligible for short waveguide runs). Eigenvalue analysis was therefore based on a tunable bandwidth of 48 to 59 GHz as well as 52 to 59 GHz.

The variation of antenna beamwidth with frequency can cause nonrepresentative sampling of the sky, especially in the presence of cloud. To obtain better retrievals, averaging or Kalman filtering of the observed data can be performed. This may be necessary in any case for elevation scans as different parts of the sky are being observed. We may consider antenna designs that have constant beamwidth across their bandwidth, but the gain in improved retrievals may be slight. Constant beamwidth feedhorns have been constructed at lower frequencies (Hogg et al., 1979, Hogg et al., 1983, Thomas et al., 1986). Such feedhorns are difficult to construct, and are therefore expensive.

(2.b) Determination of radiometer frequencies with maximum information content

Our first task in determining an optimum inversion method was to determine the nonredundant frequency ensemble that contains a maximum of information on the water vapor profile.

Rather than intuitively choosing frequency ensembles and calculating eigenvalues, we performed a more definitive search by determining and ranking eigenvalues for an ensemble of 37 frequencies spaced at 200 MHz across a 7.2 GHz tuning range.Singular value decomposition (SVD, equivalent to eigenvalue analysis) was applied in this determination. Two tuning bandwidths were selected: 22.035 to 29.235 GHz (assumed to be better for vapor profiling) and 20.035 to 27.235 GHz (deemed interesting to research the water vapor line shape and strength model parameters). Radiometrics can obtain isolator, mixer, and other receiver hardware to span either of these ranges, and can therefore build a synthesized radiometer for either range of frequencies. The frequency range options for the K band receiver are shown below in Figure 1.

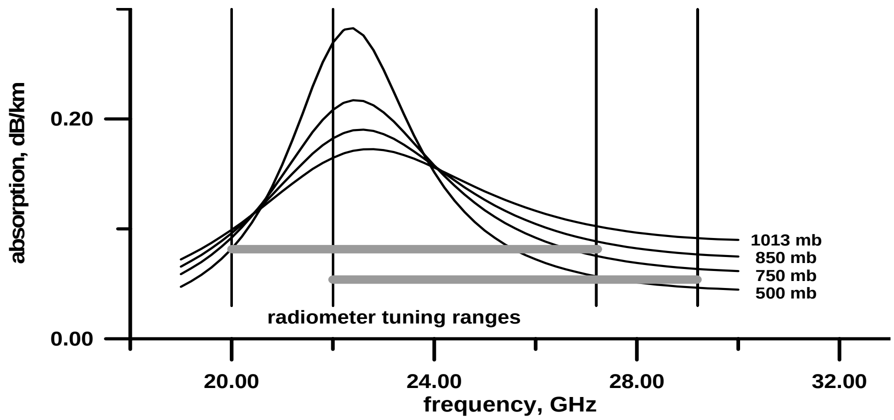

FIGURE 1. The tuning bandwidth options explored. The 20 to 27 GHz option would allow determination of the line shape and strength parameters. The 22 to 29 Ghz option yields slightly more information on the water vapor, temperature, and cloud liquid profiles.

RAOBs from Norman Oklahoma were separated into cloudy and clear conditions. This site was chosen because of its wide range of water vapor values and profile structures. Although optimum frequency ensembles are expected to differ for differing climatologies, we expect these differences to be slight. We also expect climatology to have little or no effect upon our selection of the placement of the tuning limits of the radiometer.

An average profile, based on all RAOBs, was generated and eigenvalues determined for this profile, but it was felt that the average profile was lacking in detail and structure of individual profiles, and the resultant frequency ensemble would favor smooth profiles and lack the ability to retrieve structure. So eigenvalues for *each* of about 2000 RAOB profiles were calculated using NOAA ETL's Radiative Transfer Software. For increased signal relative to the instrument error, 14.5 and 30 degree elevation angles were utilized in addition to zenith. It is envisioned that a number of observation cycles at several azimuth angles will be performed and averaged to remove gross anisotropy from the profile measurement.

As a first step in our SVD analysis, the weighting functions *W* as defined by Westwater (1993) for each of the candidate frequencies for each RAOB sounding were numerically calculated:

$$W_{\rho_v}(s) = e^{-\tau(0,s)} \frac{\partial \alpha(s)}{\partial \rho_v} \left[T(s) - T_{b_0} e^{-\tau(s,\infty)} - \int_s^{\infty} T(s') \alpha e^{-\tau(s,s')} ds' \right]$$

This was accomplished using NOAA ETL weighting function software.The weighting function specifies the brightness temperature sensitivity for a particular radiometer frequency. The eigenvalues were then determined from SVD analysis. An example of the scatter plots of the eigenvalues for all of the soundings is shown in FIGURE 2. These scatter plots determined the frequencies with maximum information content and their ranking. SVD analysis was then performed on these frequency ensembles to determine the number of independent observations contained in observations at these frequencies.

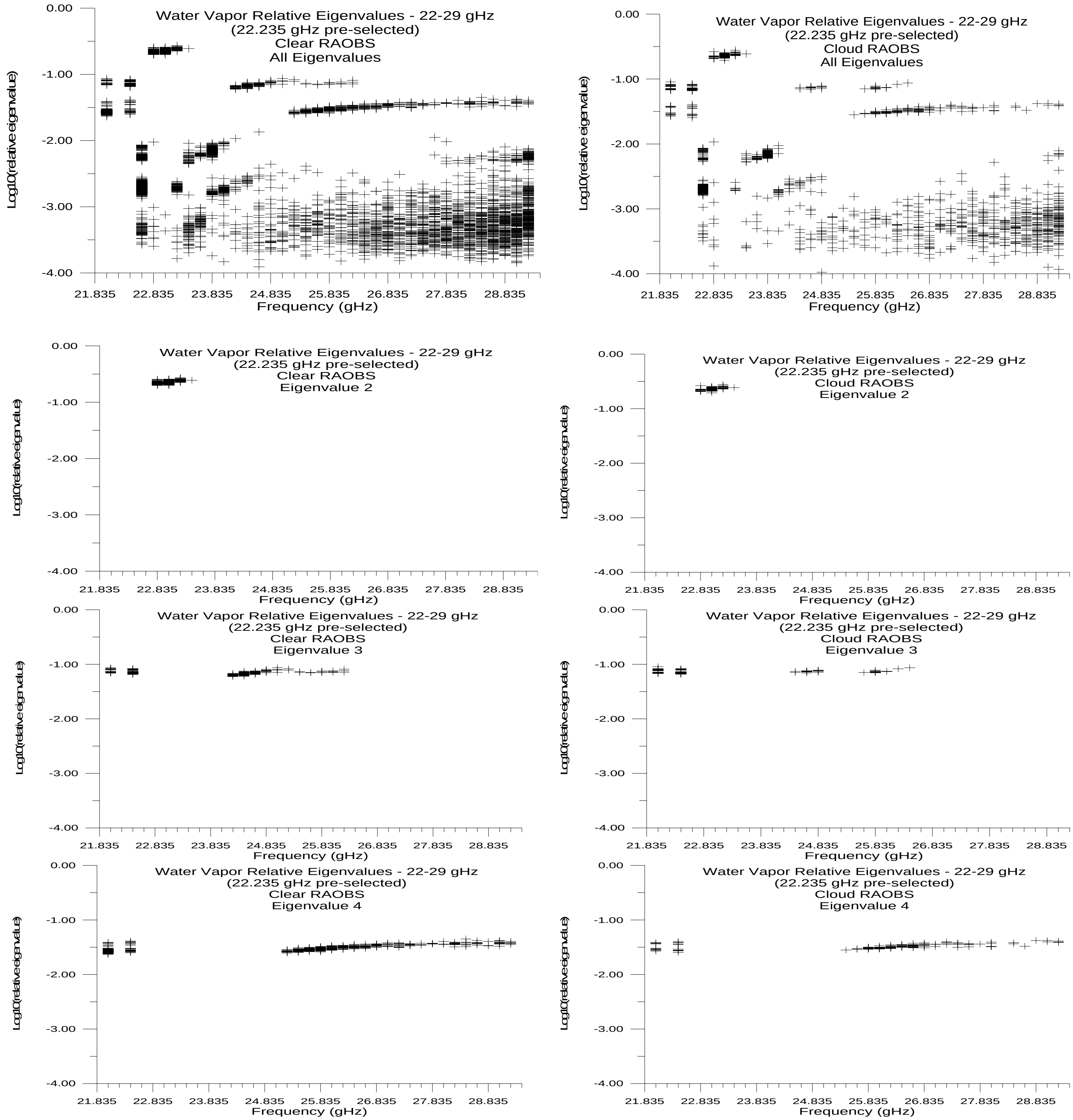

FIGURE 2. Scatter plots of water vapor profile eigenvalues for 22.035-29.235 GHz *without* 31.4 GHz, all clear cases and all cloudy cases (top two panels). Scatter plots for sequentially less significant eigenvalues (lower panels).

Westwater and Han independently performed eigenvalue analysis on the covariance matrices of brightness temperatures with matching results.

(2.c) Ancillary Information on Cloud Base Altitude and/or Temperature

As is demonstrated in a recent publication by Han and Westwater (1995), knowing cloud base altitude and temperature (and therefore water vapor density) is a very strong constraint in retrieval of water vapor profiles. This is also a strong constraint in cloud liquid profile retrieval. Such constraints greatly improve profiles above what the eigenvalues indicate.

Cloud base temperature information can be obtained from a passive IR camera. Cloud base height can be obtained from a ceilometer. Knowing the temperature profile allows either hardware method to determine both cloud base temperature and altitude. It is therefore suggested that such hardware be included with the radiometric instrument for optimum profiling ability. The cloud base temperature is important to cloud profile retrieval, and the IR camera would probably give a better measure of this temperature than determining it from ceilometer and retrieved temperature profile.

(2.d) Additional Profile Information from Historical RAOBs

With the exception of the direct retrieval method utilizing solely surface meteorological and radiometer spectral information, all of the retrieval methods incorporated statistical information on the behavior of the several profile types that was obtained from a history of RAOBs. Although the eigenvalue analysis below determines the number of independent measurements obtained from the radiometric spectral information, the ability to retrieve and resolve profiles by these methods is greatly enhanced by the statistical information. This is evidenced by the FIGURE 7., wherein sample profile retrievals are compared to the RAOB sounding and to neural network retrievals. Note the increased resolution and accuracy obtained by inclusion of climatological information.

(2.e) Multiple elevation angles vs. single elevation angle

We have determined eigenvalues for frequency/elevation angle ensembles containing three elevation angles and containing 1 elevation angle. The sky was assumed stratified in all retrieved parameters. In addition to adding to the number of eigenvalues by adding observations, there is information in the difference in brightness between elevation angles at each frequency. Because the temperature profile varies only slowly spatially (except in the vicinity of frontal and other features), the gain in eigenvalues with the use of several elevation angles is greater than the spatial noise. This results in a resultant decrease in rms retrieval noise. This is not true for water vapor because of the scale of water vapor features. We find that fourier transform of the measured spatial/temporal spectrum of water vapor reveals features of the scale of 1 km and less. Use of multiple elevation angles therefore dictates some form of averaging the observations be applied. We find, however, that the rms errors in the retrieved vapor profiles for zenith only observations and for three-angle observations are nearly the same (FIGURE 3.). This demonstrates that single-angle retrievals may be preferred to decrease the effect of inhomogeneity, and in fact, profiles could be retrieved separately for ***each*** of the elevation angles and the results compared.

The spatial inhomogeneity of cloud liquid water is more exacerbated than water vapor. However, we likewise find that single angle cloud liquid retrievals are nearly as resolute as three-angle retrievals that assume stratification.

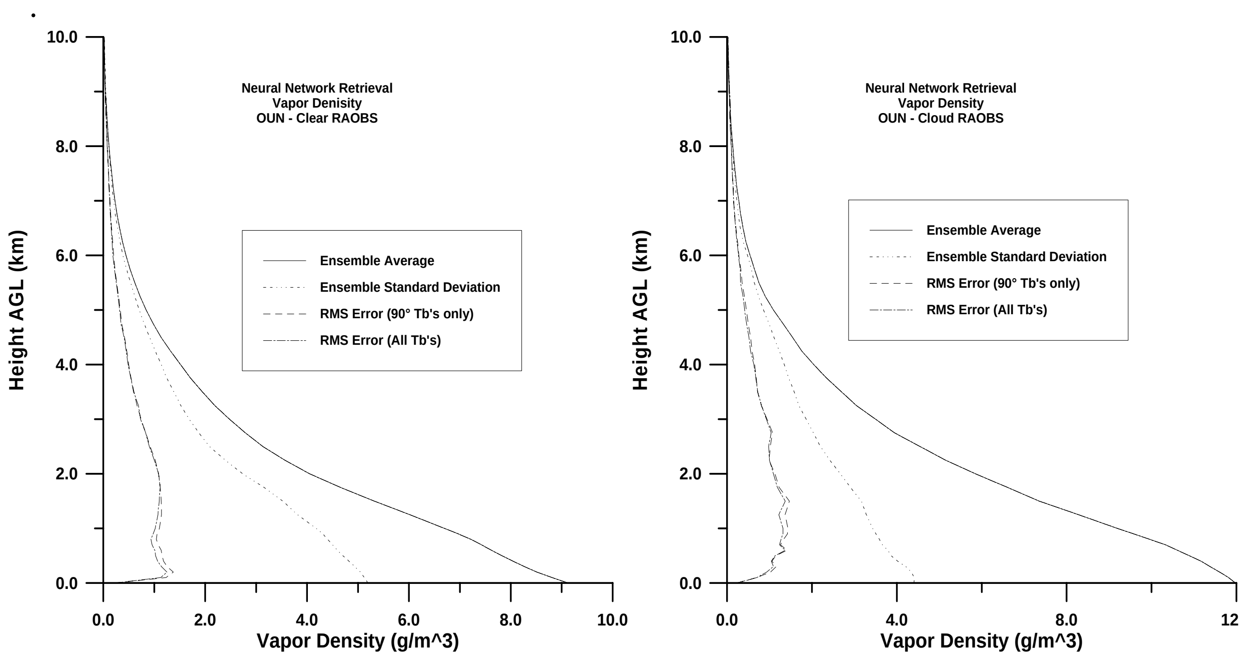

FIGURE 3. RMS errors for zenith only and for three-angle water vapor profile retrievals. Retrievals are all-season; not binned into seasons.

(2.f) Eigenvalues and frequency ensemble for the three types of profiles

In addition to the proposed analysis on the K band channels for water vapor profiling, we further undertook the SVD analysis for the following purposes.

- Water vapor profiling using the K+V bands
- Temperature profiling using the V band and using the K+V bands
- Cloud liquid water profiling using the K band and using the K+V bands
- Cloud liquid profiling using both sides of the 60 GHz oxygen feature
- Cloud liquid profiling using both sides of the 60 GHz oxygen feature and the K band

The frequency ranking in this report was accomplished as follows. Weighting functions for all frequencies at 200 MHz intervals within the tuning waveband and at elevation angles 90 (1 air mass), 30 (2 air masses), and 14.5 degrees (4 air masses) for each RAOB from Norman OK 1992 were calculated. Norman was chosen because of its wide variance in weather conditions. The frequency containing the most information (i.e. the frequency whose weighting function has the largest response integrated over altitude) was preselected (e.g., 22.235 for water vapor and 14.5 degrees when elevation angles were included in the selection process), and SVD analysis was then performed to find the eigenvalues resulting from adding each (remaining) frequency to the current frequency complement. The eigenvalues (which are all real and positive since they are from a covariance matrix) are then summed for all RAOBS and the frequency with the largest sum was then included in the frequency complement, and the process repeated to find the next frequency.

Results are summarized in tables below for profiling the three atmospheric parameters.

The existing White Sands/Radiometrics microwave temperature profiler (MTP) scans from 52.8 to 58.8 GHz. For comparison purposes and to further optimize their performance of this MTP, eigenvalue analysis to determine optimum observing frequencies was performed on this receiver tuning range.

(2.g) Frequency Ranking by Profile Information Content

The frequencies/elevations are ranked in the tables below in order of information content for each of the three profile types. These rankings should not be taken as absolute but as representative only, as they are based on Norman Oklahoma soundings and are therefore based on a specific climatology. The frequency/elevation angle ranking will slightly differ for different sites. However, ground-based weighting functions for the three atmospheric parameters considered herein are far from unique, and adjacent frequency/elevation choices are highly correlated and give essentially the same information content. Therefore, the optimal frequency/elevation ensemble for Norman is probably optimal for a wide variance of climatologies. It should also be noted that there are many possible subsets of a large, highly dependent set of weighting functions that span the same space equally well. In particular, the choice of a different preselected frequency will result in different frequency complements. The number of eigenvalues given a set cutoff will remain the same although marginal eigenvalues may drift slightly above and below the cutoff. Also, the choice of poor frequencies (i.e. those whose weighting functions are essentially zero) will cause the frequency selection algorithm to produce unpredictable results.

Sample weighting functions up to 10 km for a clear case and for a cloudy case are shown after each table of frequency/elevation rankings. Note that these weighting functions are for a single sounding and therefore have some high frequency response in some of the weighting functions due to clouds, inversions, and other profile features.

TABLE 1. Ranking of water vapor profiling preferred angle/frequency combinations. 0.5K instrument error values are above break in columns; 0.2K instrument error values include all values in columns. Boldface indicates preselected (beginning) values.

22 to 29 GHz at 14.5 deg.		**22 to 29 GHz, elevation scans**		**22 to 29 and 48 to 59 GHz, at zenith**		**22 to 29 and 48 to 59 GHz, at 14.5 deg.**		**22 to 29 and 48 to 59 GHz, elevation scans**		**22 to 29 and 52 to 59 GHz, elevation scans**	
clear	cloud	clear	cloud	clear	cloud	clear	cloud	clear	cloud	**clear**	**cloud**
22.235	**22.235**	**14.5 22.235**	**14.5 22.235**	**22.235**	**22.235**	**22.235**	**22.235**	**90.0 22.235**	**90.0 22.235**	**90.0 22.235**	**90.0 22.235**
23.035	23.035	14.5 23.035	14.5 23.035	23.035	23.035	23.035	23.035	14.5 23.835	14.5 23.635	14.5 23.835	14.5 23.635
22.435	22.035	14.5 22.435	14.5 22.035	22.435	22.435	22.435	22.035	30.0 22.635	30.0 22.635	30.0 22.635	30.0 22.635
26.235	27.035	14.5 26.235	14.5 27.035	48.220	48.220	26.236	27.035	14.5 48.220	14.5 29.235	14.5 29.235	14.5 29.235
23.835	23.835	14.5 23.835	14.5 23.835	24.035	24.035	23.835	23.835	30.0 22.035	30.0 22.035	30.0 22.035	30.0 22.035
						48.220					
22.635	22.635	14.5 22.635	30.0 22.635	53.330	52.850		22.635	14.5 26.035	90.0 51.760	90.0 52.850	90.0 51.760
				52.850	52.280	50.300	48.220	30.0 50.300	90.0 52.280	30.0 51.760	90.0 52.280
				52.280	51.760	49.780	48.740	14.5 49.780	30.0 50.730	90.0 52.280	90.0 52.850
				51.760	53.330	48.740	49.780	30.0 51.250	90.0 51.250	90.0 53.330	90.0 53.330
				51.250	51.250	49.260		14.5 48.740	90.0 52.850	14.5 23.235	14.5 24.635
				50.730	50.300	50.730		30.0 50.730	30.0 50.300	90.0 53.850	90.0 53.850
				50.300	50.730			30.0 51.760	30.0 49.260		
				49.780	53.850			90.0 52.850	30.0 24.635		

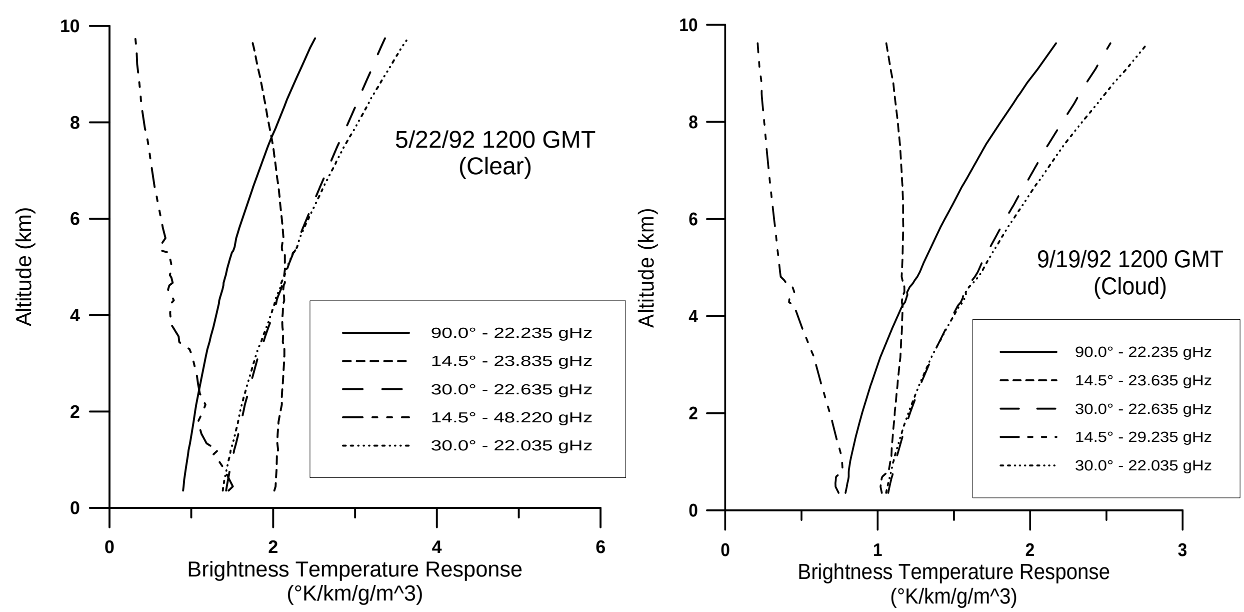

FIGURE 4. Water vapor profiling weighting functions down to first cutoff associated with the the 22 to 29 and 48 to 59 GHz elevation scanning capability (last column in the table above).

TABLE 2. Ranking of cloud liquid water profiling preferred angle/frequency combinations. 0.5K instrument error values are above break in columns; 0.2K instrument error values include all values in columns. Boldface indicates preselected (beginning) values.

22 to 29 GHz, elev. scans	22 to 29 and 49 to 59 GHz, zenith	22 to 29 and 49 to 59 GHz, 30 deg	22 to 29 and 49 to 59 GHz, 14.5 deg	22 to 29 and 49 to 59 GHz elev. scans	48 to 59 and 63 to 73 GHz, zenith	22 to 29, 48 to 59 63 to 73 GHz, elev. scans	22 to 29, 52 to 59 62 to 69 GHz elev. scans
14.5 29.235	**29.235**	**29.235**	**29.235**	**14.5 29.235**	**73.380**	**90.0 73.380**	**90.0 69.74**
14.5 22.035	52.280	50.730	48.220	30.0 49.260	48.220	14.5 24.035	14.5 22.035
	22.035	22.035	22.035	14.5 51.760	66.000	30.0 48.220	14.5 68.70
30.0 26.635	54.400			30.0 22.035		14.5 68.700	14.5 48.74
		53.330	52.850		63.800		
	56.660	54.940	54.400	14.5 53.850		14.5 65.500	14.5 65.50
						30.0 29.235	90.0 29.235

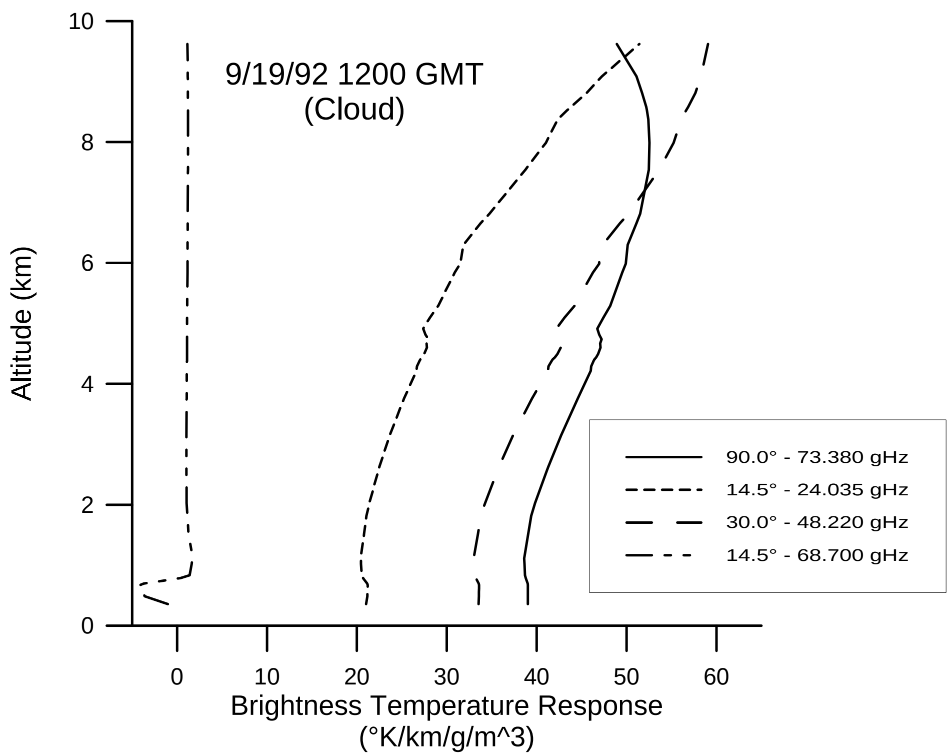

FIGURE 5. Cloud liquid profiling weighting functions associated with the 22 to 29, 48 to 59, and 63 to 73 GHz elevation scanning capability (last column in the table above).

TABLE 3. Ranking of temperature profiling preferred angle/frequency combinations. 0.5K instrument error values are above break in columns; 0.2K instrument error values include all values in columns. Boldface indicates preselected (beginning) values.

23.8 and 31.4 GHz + 48 to 59 GHz zenith		23.8 and 31.4 GHz + 48 to 59 GHz elevation scans		22 to 29 and 49 to 59 GHz zenith		22 to 29 and 49 to 59 GHz elevation scans		22 to 29 and 52 to 59 GHz elevation scans	
clear	cloud	clear	cloud	clear	cloud	clear	cloud	clear	cloud
58.80	**58.80**	**14.5 58.80**	**14.5 58.80**	**58.80**	**58.80**	**14.5 58.80**	**14.5 58.80**	**14.5 58.80**	**14.5 58.80**
54.94	48.22	30.0 56.02	14.5 54.40	54.94	48.22	30.0 56.02	14.5 54.40	30.0 56.02	14.5 54.40
56.66	54.94	90.0 54.94	14.5 31.40	56.66	54.94	90.0 54.94	14.5 29.235	90.0 54.94	14.5 29.235
50.73	56.66	14.5 56.66	90.0 54.94	50.73	56.66	14.5 56.66	90.0 54.94	14.5 56.66	90.0 54.94
	53.33	14.5 48.74	14.5 56.66		53.33	14.5 48.74	14.5 56.66		14.5 56.66
53.33			14.5 50.30	53.33			14.5 50.30	90.0 53.33	
56.02	31.4	90.0 53.33		56.02	22.235	90.0 53.33		14.5 29.235	14.5 51.76
		30.0 57.29	90.0 53.33		51.76	30.0 57.29	90.0 53.33	30.0 57.29	90.0 53.33
							14.5 22.235		14.5 22.235
							30.0 57.29		

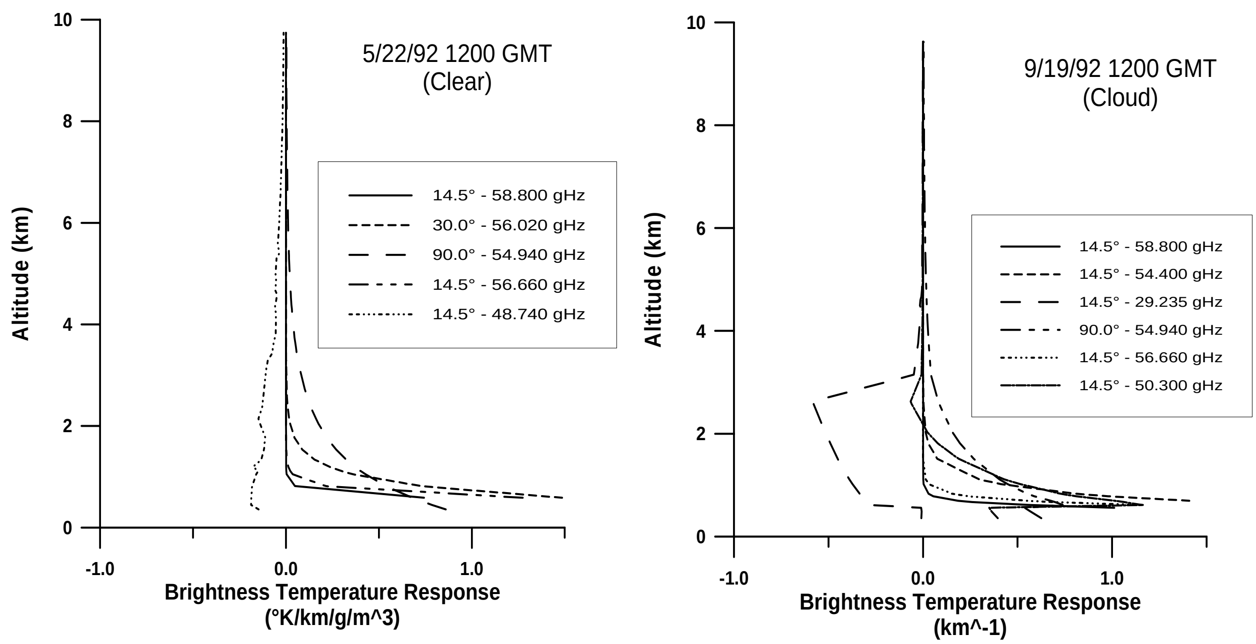

FIGURE 6. Temperature profiling weighting functions down to first cutoff associated with the 22 to 29 and 48 to 59 GHz elevation scanning capability (last column in the table above).

TABLE 4. Eigenvalues available with 7.2 GHz tuning range in the K band and 10.2 GHz the V band. Clear and cloudy condition cases yield essentially the same number of eigenvalues.

Atmospheric parameter profiled and radiometer frequency ranges	**Eigenvalues for 0.5K/100K = .005** $\left(\frac{accuracy K)}{observable(K))}\right)$	**Eigenvalues for 0.2K/200K = .001** $\left(\frac{accuracy K)}{observable(K))}\right)$
<u>Water vapor profiler</u>	clear/cloud	clear/cloud
22 to 29 GHz, elevation scans	5/5	6/6
22 to 29 GHz, 14.5 deg.	5/5	6/6
22 to 29 and 48 to 59 GHz, zenith	5/5	13/13
22 to 29 and 48 to 59 GHz. 14.5 deg.	6/5	11/9
22 to 29 and 48 to 59 GHz. elev. scans	5/5	13/13
22 to 29 and 52 to 59 GHz. elev. scans	5/5	12/12
<u>Cloud liquid profiler</u>	cloud	cloud
22-29 GHz elevation scans	2	3
22-29 and 48-59 GHz zenith	4	5
22-29 and 48-59 GHz 30 deg.	3	5
22-29 and 48-59 GHz 14.5 deg.	3	5
22 to 29 and 48-59GHz GHz elevation scans	4	5
48-59 and 63-73 GHz zenith	3	4
22-29, 48-59 and 63-73 GHz elevation scans	4	6
22-29, 52-59 and 61-68 GHz elevation scans	4	5
<u>Temperature profile</u>r	clear/cloud	clear/cloud
Existing 23.8, 31.4, and 52.85 to 58.8 GHz:		
•11 V band frequencies	5/5	6/6
•11 V band at 90, 30, 14.5 deg.	5/5	7/8
Proposed radiometer:		
23.8, 31.4, and 48 to 59 GHz, zenith	4/5	6/6
23.8, 31.4, and 48 to 59 GHz, elevation scans	5/6	7/7
22 to 29 and 48 to 59 GHz, zenith	4/5	6/7
22 to 29 and 48 to 59 GHz, elevation scans	5/6	6/9
22 to 29 and 52 to 59 GHz, elevation scans	4/5	5/8

(2.h) The frequency and elevation angle ensemble for combined temperature/water vapor/cloud liquid profiling

Eigenvalues and the associated frequency/angle combinations were determined for simultaneous profiling of water vapor, cloud liquid, and temperature. We constructed the frequency/elevation angle ensemble for our proposed water vapor profiling and for our proposed temperature/water vapor profiling instrument. Table 5 below lists the selected values for water vapor profiling.

22 to 29 GHz, elevation scans			
clear		cloud	
14.5	**22.235**	**14.5**	**22.235**
14.5	23.035	14.5	23.035
14.5	22.435	14.5	22.035
14.5	26.235	14.5	27.035
14.5	23.835	14.5	23.835
14.5	22.635	30.0	22.635

TABLE 5. Frequencies for water vapor profiling. Note that all elevation angles selected in the eigenvalue analysis are at 14.5 degrees (4 air masses).

In the case of the vapor+temperature profiler, assembling an ensemble that satisfied the eigenvalue requirements for the two different profile types to be retrieved was required. Operationally there exist biases and noise in the calibration of the radiometer receiver at each frequency. There exists information from the differences in measured brightnesses from the angular measurements at each frequency. Therefore, although there is only one elevation angle for each of the selected frequencies, we may elect to observe each of the selected frequencies at all elevation angles. Because the radiometer receiver can steer to frequencies in a few milliseconds, while the mirror elevation changes take several seconds, the instrument cycle time is not significantly increased by including all selected frequencies at each elevation angle. There is a countervailing argument, however, based on spatial variability of water vapor and cloud liquid (see Chapter 3.). The frequency ensemble for simultaneously profiling all three parameters is in Table 6 below.

TABLE 6. Frequencies for temperature , water vapor, and cloud liquid water profiling.

22 to 29 and 52 to 59 GHz elevation scans
22.035
22.235
22.635
23.835
29.235*
51.760*
52.280
54.400
54.940
56.020
56.660
58.800
*cloud liquid profiling frequencies

3. Description of the various retrieval methods tested

Ten years of RAOBs from Denver, Oklahoma City, and West Palm Beach Florida were used as the training set. The subsequent three years of RAOBs for each of these sites were used as the test set. Neural networking was applied to all three sites and all three profile types. The Bayesian method was applied to water vapor profiles at Denver. The Han/Westwater statistical regression and Newton iterative method was applied to Oklahoma temperature and water vapor profiles. The RMS errors used to corrupt the observables were 0.5° K for brightness temperatures and surface temperature, 3 mb for surface pressure, 1% for surface relative humidity and 0.1km for cloud base data (we later learned that ceilometers are considerably more accurate than this). These corrupted observables were utilized in all inversion methods tested herein.

Year-round retrievals were utilized in all cases to conserve CPU time. Had the retreivals been binned into seasons or months, we would expect a significant improvement in the rms retrieval errors (Figures 8, 9, and 10) and in the individual profiles (Appendix B).

(3.a) Han/Westwater Newtonian iteration retrieval method

Two methods developed at NOAA/ETL were applied to retrieval of profiles and associated parameters from brightness temperature and in situ surface measurements. The first is described in this section and follows the methods described in Han and Westwater (1995). The second method is described in the following section. For both methods, the simulated measurements included surface temperature, water vapor, pressure, and cloud base height as well as the 12 zenith brightness temperatures in TABLE 6. From these measurements, the following quantities were retrieved: water vapor profile, temperature profile, and integrated liquid. From the water vapor and temperature profiles, various integrated quantities can also be derived. Such quantities could include layer-averaged water vapor, precipitable water vapor, geopotential height and thickness.

The relationship between the measurements, represented by the m-dimensional measurement vector $\boldsymbol{y}$, and the quantities to be retrieved, represented by the n-dimensional profile vector $\boldsymbol{x}$, may be expressed as

$$\boldsymbol{y}=\boldsymbol{F(x)}$$

which is, in general, nonlinear. This expression may be viewed as a mapping of a profile vector in the n-dimensional profile space into the m-dimensional measurement space. The retrieval process solves the above equation and derives the profile $\boldsymbol{x}$ from the measurement $\boldsymbol{y}$. It is important to note that in the problem encountered here, for a given measurements vector $\boldsymbol{y}$, there are an infinite number of profile vectors that satisfy the above expression. Thus, a unique solution does not exit. Additional information about $\boldsymbol{x}$ is required to constrain the solution. One such information source is a statistical ensemble of a large number of historic radiosonde profiles. A technique that incorporates such a statistical constraint is the Newtonian iteration inversion method. The $(k+1)^{th}$ iteration solution can be expressed as

$$x_{k+1} = x_s + S_x K_k^T (K_k S_x K_k^T + S_e)^{-1} \left[y - y_k - K_k (x_s - x_k) \right], \quad k = 0, 1, 2, \ldots$$

where x_k is the k^{th} solution, y is the measurement vector with an error covariance matrix S_e, K_k, calculated as

$$K_k = \partial F / \partial x|_{x=x_k}$$

contains weighting functions evaluated at the k^{th} estimate x_k of x, and $y_k=F(x_k)$. The statistical constraint is represented by the x_s and S_x, the mean and covariance matrix of the statistical ensemble. Implementation of this method is the following.

The profile vector has 99 elements. The first 49 elements are water vapor density at the levels z_i=I*0.25 km, I=0,48; the next 49 elements represent temperature profile having the same vertical coordinates; the last element is the integrated liquid. The measurement vector has 14 elements. The first 12 elements are brightness temperature measurements at the specified 12 frequencies. The last two elements are surface vapor density and temperature.

The weighting functions associated with the brightness temperatures were calculated analytically using a NOAA ETL routine (see Schroeder and Westwater, 1991 and 1992). The weighting function associated with the integrated liquid is calculated using a perturbation method. In calculating the weighting functions, the integrated liquid is distributed moist-adiabatically from the cloud base.

The statistical information may be used more efficiently by the classification of the statistical ensemble according to the cloud base heights, which can be identified from the relative humidity profiles. The statistical ensemble is divided into several subensembles, each of which contains only the radiosonde profiles having the same cloud base height. For each subensemble, x_s and S_x are calculated.

The retrieval process starts with the calculation of the initial profile x_0. By using a regression method, the profile portion of the initial estimate x_0 of x is obtained from surface water vapor and temperature measurements and the integrated liquid portion is obtained from the two brightness temperatures at 23.835 and 29.235. The next step is to identify a set of $\{x_s, S_x\}_i$ by the cloud base height measurement. Then the iteration starts. For this experiment, the iteration is terminated at k=2.

(3.b) Regression retrieval method by Han/Westwater

This method uses the traditional linear statistical inversion method summarized by Westwater (1993) and Rodgers (1976). The independent vector $\boldsymbol{y}$ contains the 12 brightness temperatures, surface vapor density, and surface temperature. The dependent vector $\boldsymbol{x}$ contains the water vapor profile, temperature profile, and integrated liquid. The dependent vector is obtained linearly from the independent vector as

$$\boldsymbol{x}=\boldsymbol{a}+\boldsymbol{b}\boldsymbol{y}$$

where $\boldsymbol{a}$ and $\boldsymbol{b}$ are obtained from a statistical ensemble of radiosonde profiles using multivariate regression methods.

It is noted that the Newton iteration method explored by Han/Westwater yields slightly better results than the regression method due to the cloud base height data included in the iteration method. It is also noted that the cloud base height data utilized in the iteration method improves integrated liquid retrievals significantly in comparison with the regression method that does not use the cloud base height data.

(3.c) Neural networking

All neural networks were standard feed-forward networks with 3 layers: input, 1 hidden, and output, with full connection between adjacent layers. A standard back-propagation algorithm was used for training. The training data sets were derived from 10 years of RAOBs for each of the three sites. Depending on the size of the data set, each RAOB was corrupted by Gaussian noise 1 to 4 times to decrease the sensitivity of the network to noise in the data (the limitation on data set size was due to available computer memory - the data sets ranged in size from 7000 to 20000 soundings). During training, the data were presented in randomized order approximately 5000 times. For clear RAOBs, there were 39 input nodes: 36 brightness temperatures, surface temperature, vapor density and pressure, 39 hidden nodes and 47 output nodes representing the output profile every 0.1 km from 0 to 1 km and every 0.25 km from 1 to 10 km. For cloudy conditions the cloud base information was represented by a 1 (or two 1's if two cloud bases were present) in a set of 47 height bins (at the same heights as the output profile) for a total of 86 input nodes. These networks had 86 hidden nodes and 47 output nodes. By adding a set of short-cut connections directly from the input nodes to the output nodes this allowed the cloud base information to directly affect the corresponding output profile altitude. For cloud liquid, networks with only zenith brightness temperatures were used (these had 62 input, 62 hidden and 47 output nodes). Their performance retrieving cloud liquid was equal to the networks with all 36 brightness temperatures, confirming our eigenvalue analysis that showed both data sets contained the same number (4) of independent measurements. No seasonal data segregation was performed - we would expect improved performance if it were.

The error of the retrieved vapor density error at the surface improved from 0.4 g/m^3 to 0.3 g/m^3 for Oklahoma with RH error improved from 2% to 1%. For a perfectly trained net we would expect about 0.15 to 0.2 g/m^3 error for 1% RH measurement error for OKC average surface absolute humidity of 5-6 g/m^3.

(3.d) Direct inversion of the VanVleck line shape model

The direct inversion was performed by first calculating what is essentially a matrix of weighting functions from the expressions in Appendix A and a first guess water vapor profile (exponential decay starting at the surface vapor density). Then the pseudo-inverse of this matrix was calculated using a singular value decomposition (SVD). The SVD can actually define an infinite number of pseudo-inverses since the problem is under-determined - the weighting functions do not uniquely determine the water vapor profile. The pseudo-inverse is used with the observed brightness temperatures to calculate a correction to the water vapor profile. This process is iterated until the error between predicted and observed brightness temperatures reaches some limit. In order to obtain convergence, it was necessary to limit the number of singular values to one or two. To eliminate oscillations in the solution, it was filtered after each iteration. Unfortunately, both of these techniques tend to eliminate detail from the retrieved profile. With more singular values and less filtering the algorithm sometimes produces good results but also fails to converge on many profiles. What is needed is a way of selecting among the solutions produced by the pseudo-inverse those which are most likely. The Bayesian method described below accomplishes this selection. *A priori* information is required. An example of the value of *a priori* information to retrieval is demonstrated by the comparison between the direct inversion and neural network methods is shown in FIGURE 7.

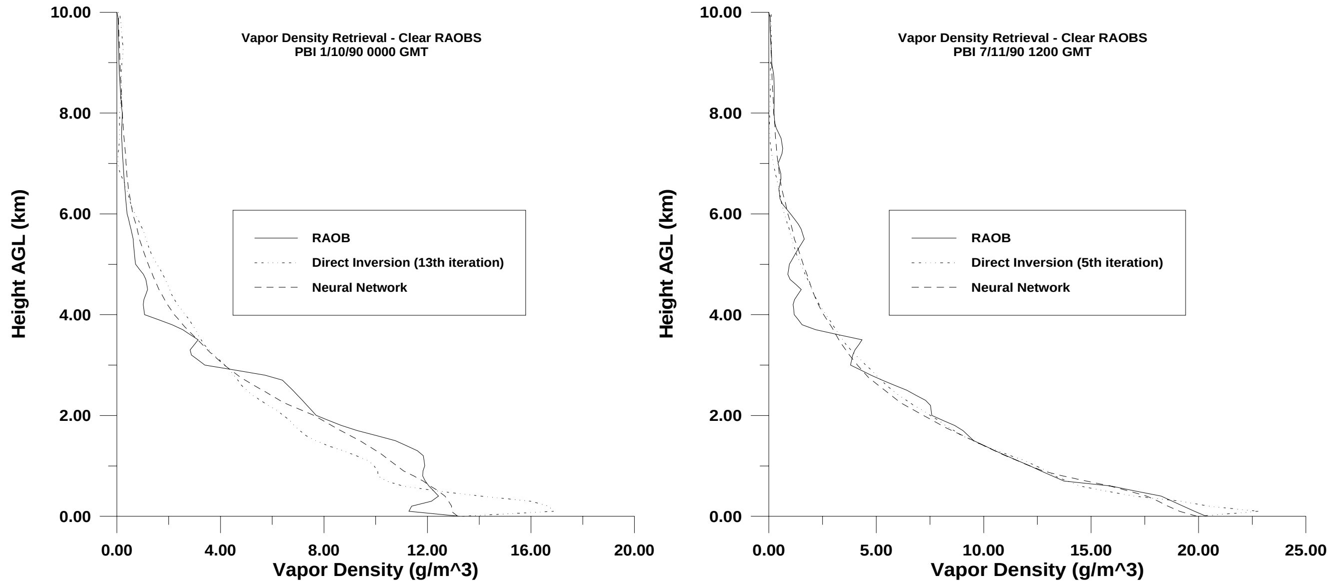

FIGURE 7. Sample direct inversion vapor density retrievals. Note the improvement of the neural network, which included *a priori* RAOB sounding data, over the direct inversion.

(3.e) Bayesian maximum probability method

The Bayesian algorithm was developed at JPL primarily for calibration of the wet tropospheric path delay during VLBI and radio science measurements such as the planned Gravitational Wave Search Experiment (GWE) using the NASA Cassini spacecraft. Simulations at JPL demonstrated the superiority of the Bayesian inversion methods over linear regression for the precise monitoring of path delay variations using microwave radiometers (Keihm and Marsh, 1996).

The model-based algorithm uses Bayes' rule to estimate the most probable value P of the state vector, **a** (e.g., vapor densities), given an observable vector, **y**, which consists of the brightness temperature measurements and surface meteorology data:

$$P(\mathbf{a}|\mathbf{y}) = P(\mathbf{y}|\mathbf{a})P(\mathbf{a})/P(\mathbf{y})$$

Gaussian statistics are assumed. The state vector, which defines the temperature and vapor density profiles over a vertical grid, is represented as a Karhunen-Loeve expansion, using eigenvectors derived from the *a priori* covariance of the state vector **a**. The state vector covariance matrix is calculated from a representative radiosonde data archive. An advantage of the Karhunen-Loeve representation is that it can reduce the number of independent unknowns. If the eigenvalues of the a priori covariance matrix are ordered by decreasing value, it often happens that only a fraction are significant; the rest represent noise. The inversion problem then reduces to estimating a smaller set of variables, the computational burden is reduced, and the accuracy of the inversion can increase if the elements of the state vector covariance matrix are not well determined from the radiosonde archive.

In practice, given a set of observables, the state vector is iterated, and the corresponding theoretical observables are computed, until the “most probable” (maximization of equation above) profile solution is obtained. In qualitative terms, the “most probable” profile solution is that which minimizes the residuals between measured and computed observables while best conforming to the constraints of the *a priori* statistics. For the current work the simulations performed on the Denver clear radiosonde data base revealed no significant advantage of the Bayesian technique for retrieval of discrete value vapor density profiles over the regression method.

4. Comparison of performance of the Retrieval Methods

(4.a) Retrieved temperature, water vapor, and liquid water profiles

The rms errors of the various retrieval methods for each of the three profile types (temperature, water vapor, liquid water) are shown in FIGURES 8, 9, and 10. The standard deviation of the parameters as measured by the RAOBs are also plotted. The rms error relative to this standard deviation indicates how much the profile is improved over an *a priori* mean profile. The average profile is also plotted to show fractional errors in the retrieved values.These retrievals were based on all-season retrievals; a better result (lower rms errors) would have been obtained if the retrievals had been binned into seasons or months.

With the exception of the VanVleck inversion, the retrieval methods tested are roughly equivalent. Neural networking demonstrated a superior ability to resolve high frequency features. In terms of temperature retrievals, the performance of the various algorithms is comparable. Excellent retrieval performance is generally found for non-inversion and ground based inversion profiles. Elevated inversions at the 0.5 km level or higher are generally smoothed in the algorithm solutions. Retrieval error rms values generally range from 1-2 K over the 1-5 km height intervals for the three sites' simulations. The standard deviation of the profiles in the RAOB ensemble (inherent variability) is the measure of rms error in simply choosing a mean profile. Relative to the inherent variabilty of temperature, the tested observational system typically provides factor of 4-6 improvement in estimation accuracy over the 1-5 km range. An exception to this relative performance improvement is found in the West Palm Beach temperature retrievals above 3 km, due to the low inherent variability of temperatures at this site. The temperature retrieval performance degrades only slightly for cloudy (versus clear) conditions with the most significant differences found at the Oklahoma site.

With the exception of the direct retrieval based on the VanVleck pressure broadening model, the various water vapor profiling algorithm performances were also comparable. Vapor density retrieval accuracies better than 1 gm/m^3 were generally obtained at all sites and altitudes. Drier sites (such as Denver) exhibit ~ 0.6 g/m^3 errors or less at all altitudes. Relative to the inherent variability at each site, the algorithm retrieval errors showed a factor of ~ 5 improvement for Denver and Oklahoma and a factor of ~ 2-3 improvement for the West Palm Beach simulations over the 0-3 km height range (where most of the water vapor resides). Only slight degradation in retrieval accuracy occurred for cloudy conditions. Elevated vertical structure on scales of ~ 1 km or is generally smoothed by the algorithm vapor profile retrievals, consistent with the expectations based on the eigenvalue analysis for the simulated observational system.

Cloud liquid profile improvements are not as dramatic, but this is due in part to the structure of clouds. Slight altitude offsets in profile features between the actual and retrieved profiles can induce large rms errors when the retrieved parameter is changing rapidly with altitude. This is especially true of highly layered profiles such as cloud liquid water where the densities can change abruptly with altitude at the cloud margins (see the cloud liquid retrieval rms error plots, Figures 8, 9, 10). The rms error evaluations are therefore not highly representative of ability to retrieve layered structure. We have therefore included a large number of individual profile retrievals in Appendix B for a subjective demonstration and comparison of retrieval capability.

(4.b) Improvement of retrieved *total integrated* water vapor and liquid water

There is a need for high precision measurement of total integrated liquid water and water vapor values for propagation delay determination for geodesy and other applications. Therefore, the effect of the number of brightness temperature observables upon retrieval of coarse resolution (1 km slab thickness) and total integrated liquid water and water vapor were investigated. The effect upon the total integrated vapor value for Denver clear RAOB cases is shown in TABLE 7. below. Note that the reduction in rms errors approximately follows a square root law on the number of observables, as might be expected if statistical reduction of noise is the determining factor. Additionally, there is some information on the distribution of water vapor along the temperature profile contained in the spectral brightness observables; because the brightness depends upon the physical temperature of the water vapor as well as its density, knowledge of its temperature can give a better retrieval. The Bayesian method may be taking advantage of this; further investigation is necessary.

TABLE 7. Total integrated vapor rms errors, cm, for clear Denver soundings.

	linear regression (Han/Westwater	**Bayesian max. prob. (Keihm/Marsh)**	**Neural networking (Godwin)**
Training set (16765 soundings)			
2 channels (23.835, 29.235) at zenith	0.036		
5 channels at zenith	0.026		
12 channels at zenith	0.022		
24 channels (zenith+air mass = 2)	0.016		
36 channels (zenith + air mass=2 & 3)	0.012		
Verification set (~2000 soundings)			
12 channels, zenith	0.015		
24 channels (zenith+air mass = 2)	0.012		
36 channels (zenith +air mass=2 & 3)	0.010	0.011	0.029

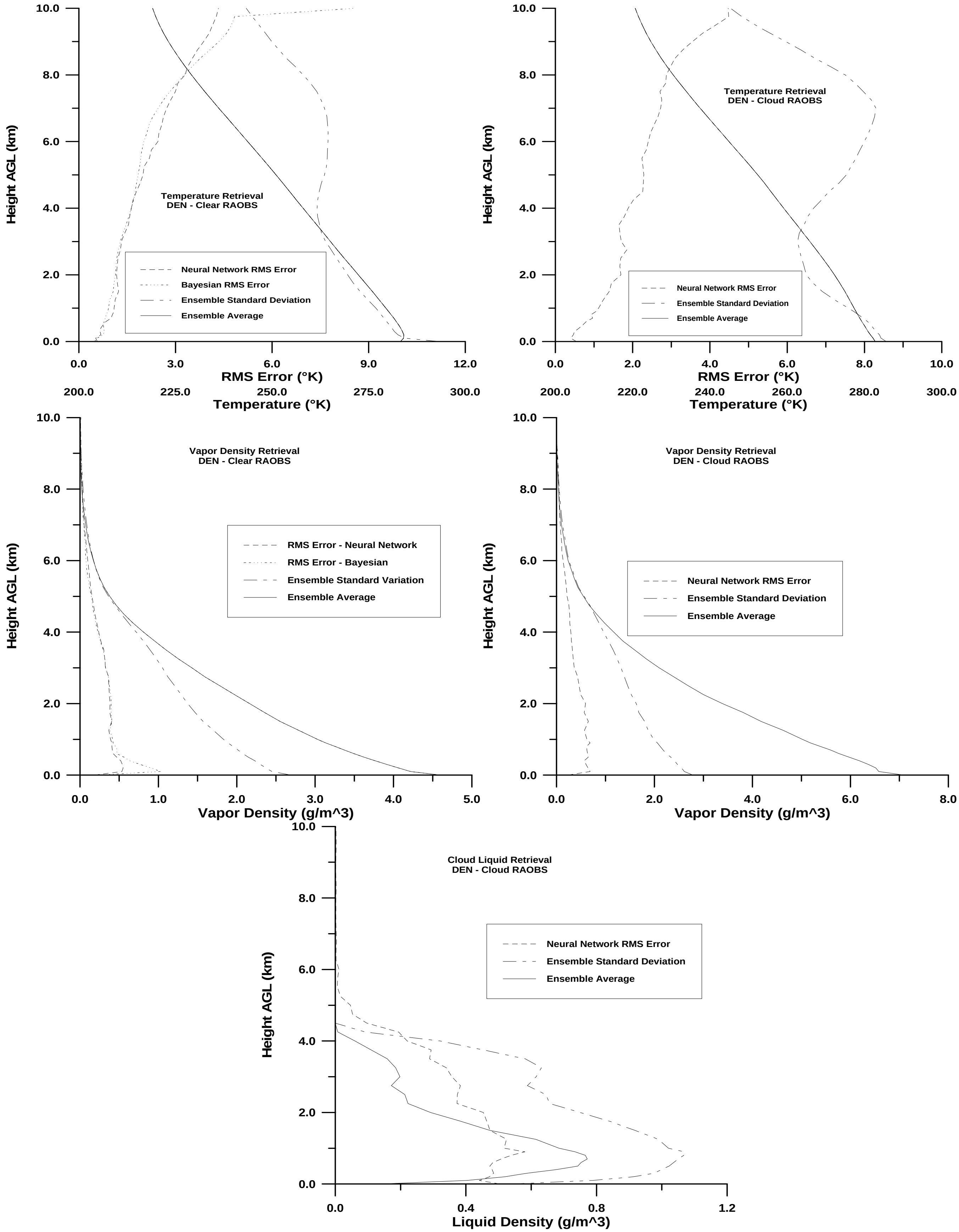

FIGURE 8. Comparison of neural network and Bayesian rms errors for Denver all-season retrievals. Binning the retrievals seasonally would significantly reduce the rms errors. The profile variances from the RAOBs and the average profile are also shown.

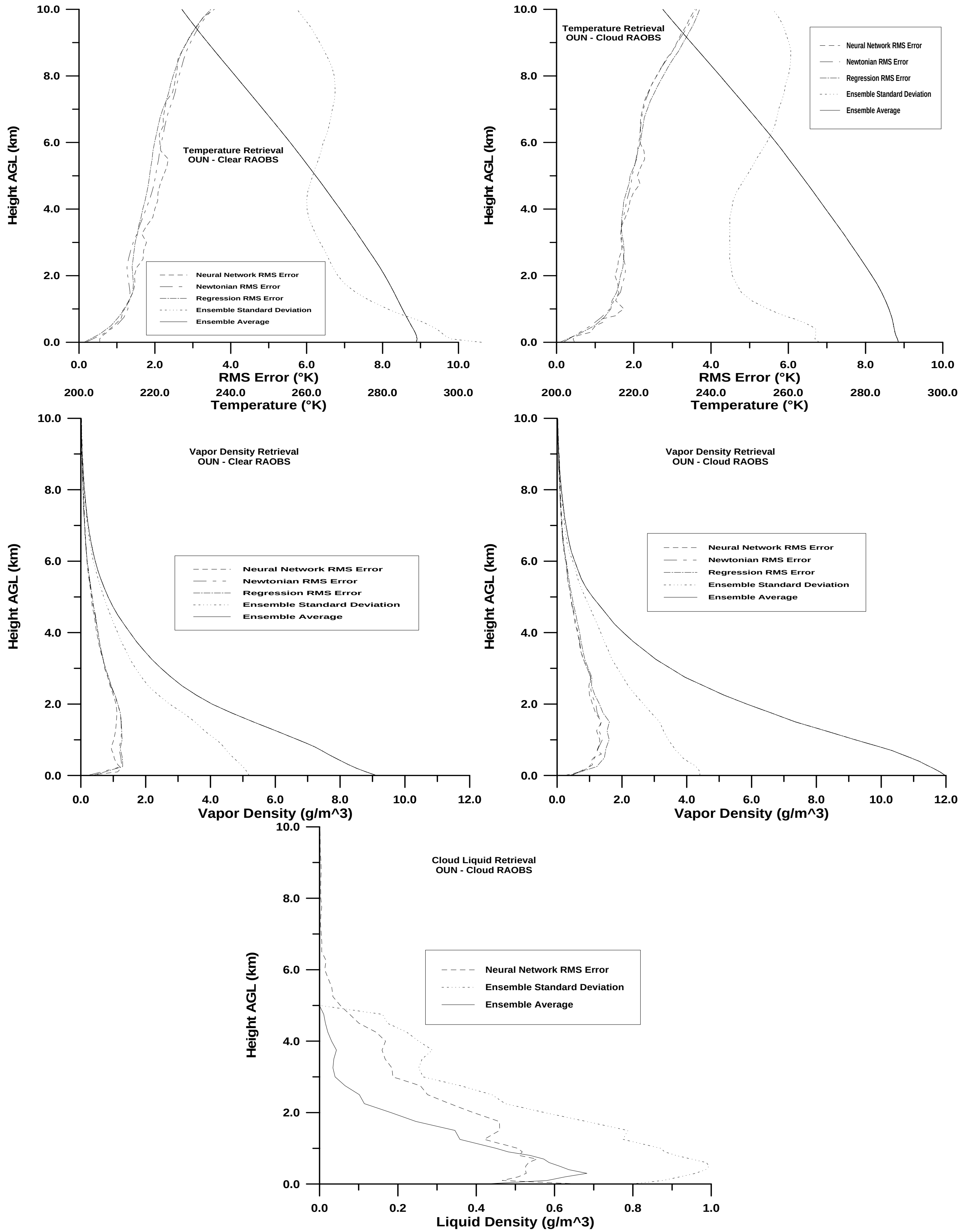

FIGURE 9. Comparison of neural network, Newtonian, and statistical regression rms errors for Norman Oklahoma all-season retrievals. The profile variances from the RAOBs and the average profile are also shown.

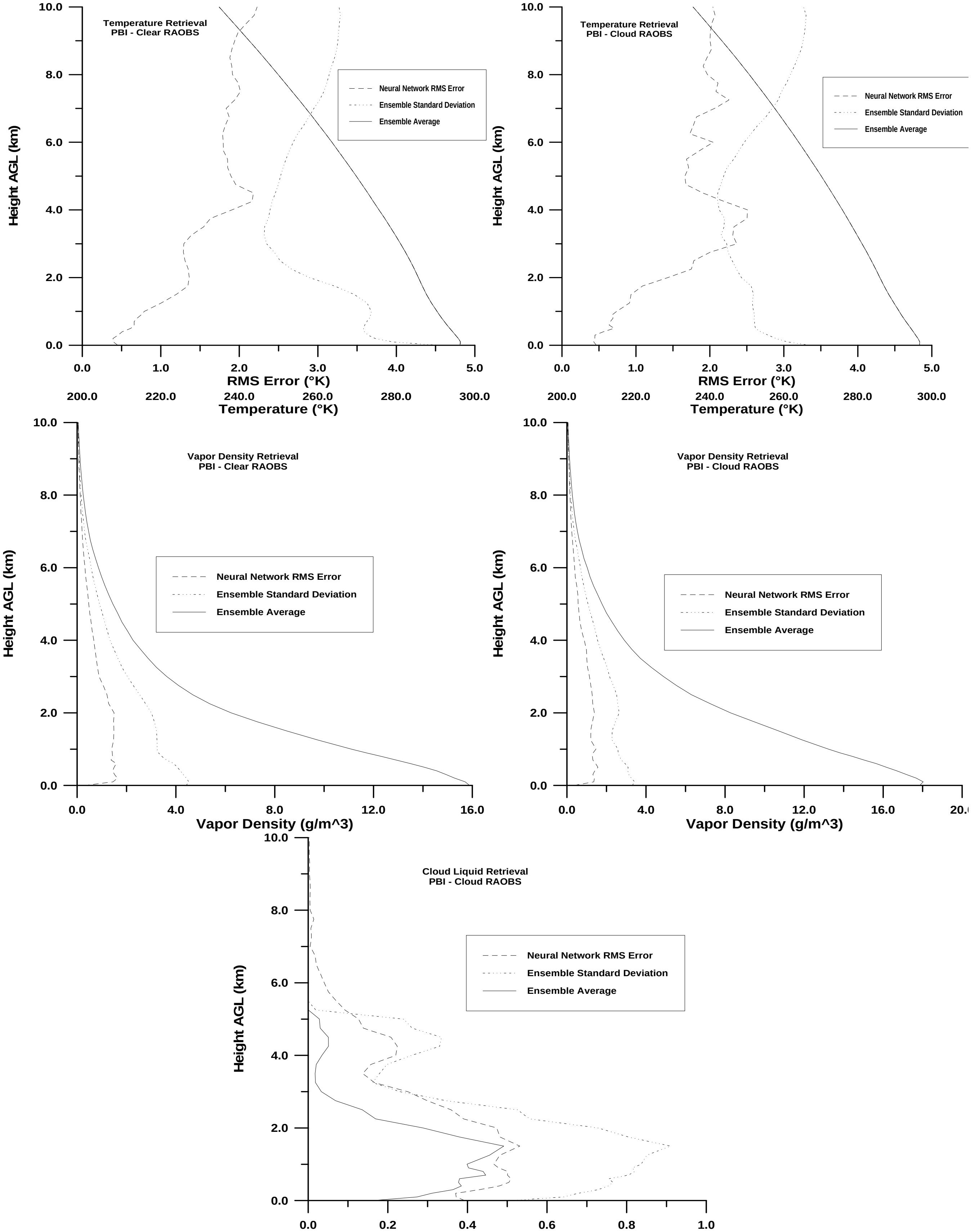

FIGURE 10. Neural network rms errors for West Palm Beach Florida all-season retrievals. The profile variances from the RAOBs and the average profile are also shown.

5. Design of the advanced profiler

(5.a) Instrument sequence and cycle time

For the water vapor profiler, the envisioned observation scheme is as follows (all six selected frequencies at each observation angle):

- •blackbody
- •blackbody + noise diode
- •air mass = 4, left side of instrument
- •air mass = 4, right side of instrument
- •blackbody
- •blackbody + noise diode

The blackbody measurements are repeated to average instrument gain and offset drift. Instrument cycle time is about 1.2 minutes.

For the water vapor + temperature profiler + cloud liquid profiler, the proposed observation scheme is to observe all twelve selected frequencies at 1, 2, and 4 air masses (90, 30, and 14.5 degrees) in the following routine:

- •blackbody
- •blackbody + noise diode
- •air mass = 1, zenith
- •air mass = 2, left side of instrument
- •air mass = 4, left side of instrument
- •air mass = 1, zenith
- •air mass = 2, right side of instrument
- •air mass = 4, right side of instrument
- •blackbody
- •blackbody + noise diode

Estimated instrument cycle time for 1 second observations at each frequency is about 3 minutes.

(5.b) IF bandwidth of the water vapor profiler

The IF bandwidth of the Radiometrics two channel WVR-1100 total integrated water vapor and liquid water radiometer is 400 MHz edge to edge, with 100 MHz straddling line center excluded to eliminate Gunn oscillator phase noise. The water vapor profiler will use a low phase noise tunable frequency synthesizer rather than Gunn oscillators, allowing the excluded centerband to be narrowed to 10 MHz or so.

The theoretical resolution of the radiometer is: $$\Delta T = \frac{Tsys}{\sqrt{B\tau}}$$

where *Tsys* is the receiver equivalent temperature, *B* is the IF bandwidth, and τ is the observation time. The loss in resolution of the radiometer due to the narrowed bandwidth can be recovered by proportionately longer observation times. Not considered in this equation are the gain and offset drift of the receiver during the instrument observation cycle, the repeatability of the noise diode gain reference, and other observational noise. Actual measurements of the WVR-1100 demonstrate a resolution of about 0.2K, about twice the theoretical value above.

Whereas the WVR-1100 receives portions of the spectrum with very little curvature as a function of frequency, the water vapor profiler will scan portions of the spectrum with significant curvature. Because of finite IF bandwidth, this curvature skews the brightness observations toward the hinge point at 23.8 GHz, and the amount of skew is dependent upon brightness (water vapor). We will therefore narrow the IF bandwidth to minimize this observational bias, and increase the spectral resolution of the receiver. The criterion we use is that the skew at the most aggravated point in the spectrum for a very wet sky be less than the resolution, delta T, of the radiometer. This determination was accomplished by numerically integrating (averaging) the antenna brightness for a wet sky between frequencies equidistant from a line centered at 22.7 GHz (a region of maximum curvature) until the difference between this average and the line center exceeds 0.2K. We find that we can utilize an edge-to-edge bandwidth of 250 MHz without incurring a bias in excess of the targeted instrument resolution.

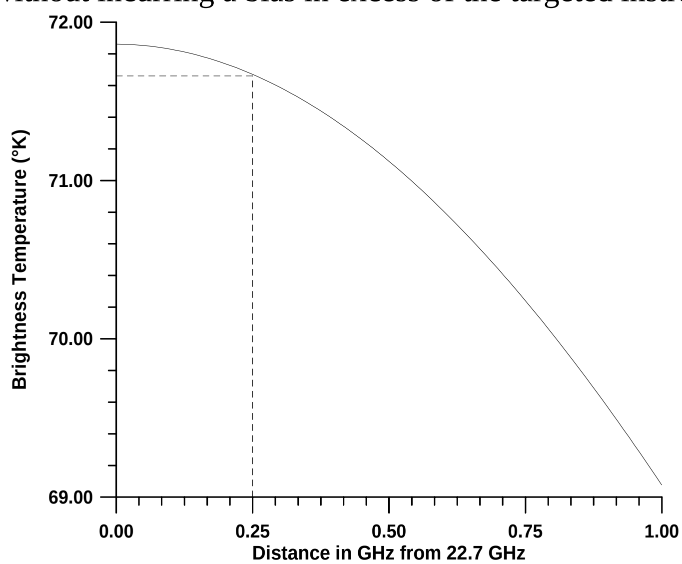

FIGURE 11. Brightness temperature as function of IF bandwidth at 22.7 gHz for a wet RAOB. Dotted lines show 250 MHz bandwidth results in about 0.2 °K change from brightness temperature at center frequency.

(5.c) MMIC Technology

We have investigated the applicability of a commercially produced MMIC transceiver to radiometer applications. This receiver has a noise figure well under 4 dB, whereas our current waveguide K band (23.8 & 31.4) receiver has a noise figure of about 5 dB. This equates to a receiver system temperature of about 350K as opposed to 630K. Current production operates from 38.6 to 40 GHz and has a 140 MHz IF bandwidth. Our radiometer design would require a bandwidth of about 100 MHz. Development is proceeding on a K band (28 GHz transceiver; the receiver of this transceiver is a candidate for a frequency agile water vapor profiler). The receiver consumes 11 watts, comparable to our current Gunn-based total integrated water vapor radiometer, but occupies about 6 cubic inches as compared with 60 cubic inches of our current receiver front end.

The manufacturer feels that this MMIC receiver design can be modified to frequency agile radiometer applications. This would require eliminating automatic gain control, addition of amplification between the antenna and receiver, and detection of the IF output of the current receiver. The result would be a lower cost, smaller, and more robust radiometer. Radiometrics is discussing a sourcing arrangement with the manufacturer.

6. Conclusions and further findings resulting from this Phase I effort

(6.a) Conclusions regarding the inversion methods

In addition to the ability of the inversion methods to accurately retrieve temperature and water vapor profiles, we found through eigenvalue analysis and through application of neural network inversion methods that we can retrieve **profiles of cloud liquid.** No other passive remote sensing technologies can accomplish this; radar techniques function only with dense and precipitating clouds.

Inclusion of statistical information into the inversion process from a history of RAOBs greatly increases the accuracy and resolution of the retrieved profiles (see FIGURE 7.). The number of eigenvalues contained in the radiometric spectral information therefore does not truly reflect (significantly underestimates) the resolution and accuracy attainable when statistical/historical information is included.

Spatial variability in the sky, especially for vapor and cloud liquid retrievals, can induce large retrieval errors if multiple elevation angles are utilized. However, we find that retrievals utilizing the **three elevation angles** (90, 20, and 14.5 degrees) only slightly reduce the rms errors in the retrieved profiles relative to utilizing zenith only observations. Also, a separate profile can be retrieved from each elevation angle.

There are **no great differences** in the ability of the various inversion methods that include statistical information to retrieve profiles of temperature, water vapor, and cloud liquid water.

Improved **total integrated** values of liquid water and water vapor are realized by the radiometer design herein over two channel radiometers, presumably because of the greater number of observables. Additionally, the Bayesian method outperformed the other techniques tested in retrieving total integrated vapor. It is thought that the Bayesian method may better determine water vapor density relative to the temperature profile, yielding a better estimation of the vapor density from the brightnesses.

(6.b) Conclusions regarding the hardware for the proposed radiometer receiver

(6.b.1) The waveguide receiver

We have identified and investigated sources of microwave components necessary to constructing a radiometer receiver capable of tuning **22 to 29 GHz**. These components include a broadband biased mixer, antenna isolator, Moreno crossguide coupler for the noise diode reference, and gaussian optical antenna. This tuning also requires a frequency agile local oscillator. We identified a highly stable synthesized LO system that is capable of this tuning bandwidth, and with sufficient output power.

We have analyzed the observation requirements, and estimate the water vapor profiling instrument **cycle time** at **less than 2 minutes**.

We estimate the water vapor profiling instrument to have the physical specifications shown in TABLE 8.

TABLE 8. Expected specifications of the water vapor profiler

Profiler function or parameter	
Sample time	User selectable for all instrument functions
Cycle time	< 2 minutes
Resolution	0.25K
Accuracy	0.5K
Size	50x28x76cm
Weight	20 kg
Power	100 watts max 110 or 220 vac, 50 to 440 cps
Environmental	-20 to +50C 0 to 100% RH noncondensing
Sky coverage	all sky
Data output (to screen and data file)	water vapor profiles (g/m^3) to 10 km

(6.b.2) MMIC receiver

Radiometrics is entering into an agreement with a manufacturer of MMIC millimeter wave and microwave transceivers to develop a MMIC radiometer. Radiometrics has recently obtained a 38 GHz transceiver for testing of gain and offset stability. This manufacturer is currently developing a 28 GHz transceiver. Although this transceiver only tunes 1.5 GHz, the design of the receiver may be amenable to broadening to a 6 or 7 GHz tuning bandwidth. A radiometer based on this MMIC receiver would be **smaller, more robust, and less costly** than the existing waveguide technology.

7. Bibliography, References

Alishouse, J.C., L.J. Krone, H.E. Fleming, F.L. Van Cleef, and D.Q. Wark, *A discussion of empirical orthogonal functions and their application to vertical temperature profiles*, **Tellus XIX** 3, 1967.

Churnside, J. H., T. A. Stermitz, and J.A. Schroeder, *Temperature Profiling with Neural Network Inversion of Microwave Radiometer Data*, **JOAT 11**, No. 1, February 1994.

Clifford, S.F., J.C. Kaimal, R.J. Lataitis, R.C. Strauch, *Ground-based Remote Profiling in Atmospheric Studies: An Overview*, **Proc. IEEE, 82**, No. 3, March 1994.

A. Deepak, *Inversion Methods in Atmospheric Remote Sounding*, Academic Press, New York, 1977.

Han, Yong and E. R. Westwater, *Remote Sensing of Tropospheric Water Vapor and Cloud Liquid Water by Integrated Ground-based Sensors*, **JAOT 12**, pp 1050-1059, October 1995.

Hogg, D, F.O. Giraud, Joe Howard, Allen C. Newell, Douglas P. Kremer, and Andrew G. Repjar, *An Antenna for Dual-Wavelength Radiometry at 21 and 32 GHz,* IEEE Antennas and Propagation AP27, p. 764, 1979.

Hogg, D., F.O. Giraud, J.B. Snider, E.R. Westwater, *A steerable dual-channel microwave radiometer for measurement of water vapor and liquid in the troposphere,* Jour. App. Met 22, #22, pp 789-806, May 1983.

Holstrom, Ingemar, *On a method for parametric represenation of the state of the atmosphere*, Tellus XV, 2, 1963.

Keihm, S.J. and K.A. Marsh (1996) Advanced algorithm and system development for Cassini radio science tropospheric calibration. Progress Report for the JPL Telecommunications and Data Acquisition Program, in preparation.

Measure, E., Y.P. Lee, T.L. Barber, and W.R. Watkins, *Neural network for retrieval of indirectly measured information*, **SPIE 1688**, Atmospheric Propagation and Remote Sensing, 1992.

Measure, Edward M., Teddy L. Barber, and Young P. Lee, *Number of Nonredundant Frequencies for Ground-Based Microwave Radiometric Temperature Profiling,* **JAOT 6**, pp 846-850, October 1989.

Rodgers, C. D., *Retrieval of Atmospheric Temperature and Composition From Remote Measurement of Thermal Radiation*, Rev. Geophys and Space Physics Vol 14, No. 4, pp 609-624, November 1976.

Rodgers, Clive D., *Characterization and Error Analysis of Profiles Retrieved From Remote Sounding Measurements*, Jour. Geophys. Res Vol. 95, No. D5, pp 5587-5595, April 20, 1990.

Schroeder, J. A., and E. R. Westwater, *User's Guide to Microwave Radiative Transfer Software,* NOAA Technical Memorandum ERL WPL-213, October 1991.

Schroeder, J. A., and E. R. Westwater, *Guide to Microwave Weighting Function Calculations*, NOAA Technical Memorandum ERL WPL-225, July 1992.

Thomas, B. MacA., G. L. James, and K.J. Greene, *Design of Wide-Band Corrugated Conical Horns for Cassegrain Antennas*, IEEE Trans Antennas & Propagation, Vol. AP-34, June 1986, pp. 750-757

Twomey, S., *Introduction to the Mathematics of Inversion in Remote Sensing and Indirect Measurements*, Elsevier Scientific Publishing, 1977.

Twomey, S., *Information Content in Remote Sensing*, **Applied Optics 13**, No. 4, April 1974.

Westwater, E. R., *Ground-Based Passive Probing Using the Microwave Spectrum of Oxygen*, Radio Science Vol. **9D**, No. 9, September 1965.

Westwater, E.R., 1993: *Ground-based Microwave Remote Sensing of Meteorological Variables,* Chapter 4 in Atmospheric Remote Sensing by Microwave Radiometry, M. Janssen, editor, J. Wiley & Sons, NY, 1993, pp. 145-213.

Appendix A

Retrieval of the atmospheric water vapor density profile by direct inversion of the pressure broadened water vapor emission line shape as received at the radiometer antenna

By Chandrasekhar's radiative transfer equation, the radiometer signal at the antenna (called "brightness temperature," T_b) as a function of frequency is:

$$T_b(f) = T_c(f)exp(-\tau_\infty(f)) + \int_0^\infty T(h)\alpha(f,h)exp(-\tau_h(f))dh \tag{1}$$

where $\tau_h(f)$ is the total opacity from the surface to h:

$$\tau_h(f) = \int_0^h \alpha(f,h')dh' \tag{2}$$

where $\alpha_t(f,h)$ is the total of all resonance and continuum absorptive constituents:

$$\alpha_t(f,h) = \alpha_{O_2}(f,h) + \alpha_v(f,h) + \alpha_c(f,h) + \alpha_i(f,h) + \alpha_a(f,h) + \ldots \tag{3}$$

The subscripts $_{O_2,v,c,i,}$ and $_a$ are for oxygen, water vapor, cloud liquid, ice, and aerosols. We shall assume the cosmic contribution $T_c(f)$ is independent of frequency across our waveband of interest. In the following we shall also drop the f subscript to simplify notation; frequency dependence is implied in all expressions for brightness, absorption, and opacity. The absorption line shape $\alpha_v(h)$ of water vapor is a function of pressure broadening, as is discussed below. This pressure broadening is the basis of altitude information on the water vapor distribution.

We write Chandrasekhar's equation as a single-frequency equation with a discrete sum over h levels replacing the integral. The discrete sum is because the integrals require numerical solutions and therefore require summations.

$$T_b \simeq T_c exp(-\tau_\infty) + \sum_{h'=0}^{\infty} T'_h \alpha_{t,h'} exp(-\tau_{h'})\delta h'$$

$$\simeq T_c exp(-\sum_{h=0}^{\infty} \alpha_{t,h}\delta h) + \sum_{h=0}^{\infty} T_h \alpha_{t,h} exp(-\sum_{h'=0}^{h} \alpha_{t,h'}\delta h')\delta h \tag{4}$$

where

$$\tau_h = \sum_{h'=0}^{h} \alpha_{t,h'}\delta h' \tag{5}$$

and the total absorption $\alpha_{t,h}$ is the sum of the contributions to oxygen, water vapor, cloud liquid, ice, aerosols, and other absorbers:

$$\alpha_{t,h} = \alpha_{O_2,h} + \alpha_{v,h} + \alpha_{c,h} + \alpha_{i,h} + \alpha_{a,h} + \ldots \tag{6}$$

We will initially consider the clear air case (oxygen and water vapor absorption), and may later include cloud liquid.

The tropospheric Van-Vleck Weiskopf line shape models

The Liebe (1993) implementation of the Van-Vleck Weiskopf line shape model is below. Other models not considered here include the Gross (kinetic) model and the model of Ben-Reuven. The vapor *continuum* must also be considered because of its magnitude, especially in the 51-59 GHz band of the radiometer.

Liebe's (1993) implementation of Rosenkranz's modification to the VV-W water vapor line shape expressing the absorptive component of the line shape factor $F(f, f_o)$ is:

$$F_v'' = f\Big[\frac{\gamma}{(f - f_o)^2 + \gamma^2} + \frac{\gamma}{(f + f_o)^2 + \gamma^2}\Big] \tag{7}$$

where f_o is the line center frequency, and the double prime indicates the imaginary (absorptive) component of the line shape factor. The line strength factor is:

$$S = e\theta^{3.5}\frac{b_1}{f_o}exp\big(b_2(1-\theta)\big) = 1.384q\theta^{2.5}\frac{b_1}{f_o}exp\big(b_2(1-\theta)\big)\ kHz/GHz\ (or\ ppm) \tag{8}$$

because $q(g/m^3) = 0.7223e(mb)\theta$, and where $\theta = 300/T(K)$. Now, the imaginary (absorptive) component of refractivity of a single water vapor resonance is:

$$\begin{aligned} N_v'' &= SF'' + continuum \\ &= 1.384q\theta^{2.5}\frac{b_1}{f_o}exp\big(b_2(1-\theta)\big)F_v'' + f(0.357\theta^{7.5}e + 0.0113\theta^3 p)e \times 10^{-6} \\ &= 1.384q\theta^{2.5}\frac{b_1}{f_o}exp\big(b_2(1-\theta)\big)F_v'' + f(0.684\theta^{5.5}q^2 + 0.0156\theta^2 pq) \times 10^{-6} \end{aligned} \tag{9}$$

Although the following derivation is for a single line, we will sum over all significant lines: $N_v'' = \sum_i S_i F_i''$. The first term on the r.h.s of (9) is the absorption due to the resonance and the second term is due to the water vapor continuum. The absorption profile is (1 dB power=0.2303 neper (np)):

$$\begin{aligned} \alpha_{v,h} &= 0.1820fN_v''\ (dB/km) = 0.04191fN_v''\ (np/km) \\ &= 0.05801q\theta^{2.5}b_1\frac{f}{f_o}exp\big(b_2(1-\theta)\big)F_v'' + f^2(287\theta^{5.5}q^2 + 6.54\theta^2 pq) \times 10^{-10}\ (np/km) \end{aligned} \tag{10}$$

$$\begin{aligned} \alpha_{v,h} = 0.05801b_1q\theta^{2.5}exp\big(b_2(1-\theta)\big)\frac{f^2}{f_o}\Big[\frac{\gamma}{(f - f_o)^2 + \gamma^2} + \frac{\gamma}{(f + f_o)^2 + \gamma^2}\Big] \\ + f^2(287\theta^{5.5}q^2 + 6.54\theta^2 pq) \times 10^{-10}\ np/km \end{aligned} \tag{11}$$

The pressure broadening half-width (γ) of Liebe (1993) is as above:

$$\begin{aligned} \gamma &= (b_3 \times 10^{-3})(p\theta^{b_5} + b_4 e\theta^{b_6}) = (b_3 \times 10^{-3})(p\theta^{b_5} + 1.384b_4 q\theta^{b_6 - 1}) \\ &= (b_3 \times 10^{-3})(p\theta^{b_5} + 1.384b_4 q)\ GHz \end{aligned} \tag{12}$$

because $b_6 = 1$. The pressures (p and e) are in millibars and q is in g/m^3. This pressure broadening expression is valid to about 60km, where Doppler broadening becomes significant.

The emission in this frequency regime for a non-scattering atmosphere is:

$$I(f,h) = \alpha(f,h)T(h) = T(h)\sum_{f_o} S_{f_o}(T)F''(f,f_o)$$

where $S_{f_o}(T)$ is the line strength as above.

An iterative method

The above functional forms are not amenable to linearization with any precision. I therefore investigate an iterative method based on a matrix of partial derivatives. Note that these partial derivatives are related to the weighting functions. To find the dependence of the line shape upon water vapor concentration at any given altitude, we will determine the derivative of equation (3) w.r.t. $q(h)$:

$$\delta T_b(f) = \frac{\partial T_b(f)}{\partial q(h)}\delta q(h) \ or \ \delta \vec{T}_{b,f} = \underline{\left|\frac{\partial T_{b,f}}{\partial q_h}\right|}\delta \vec{q}_h \tag{13}$$

in matrix notation. This will allow us to adjust the vapor profile at various altitudes to match an observed line shape profile by utilizing:

$$\delta \vec{q}_h = \underline{\left|\frac{\partial T_{b,f}}{\partial q_h}\right|}^{-1}\delta \vec{T}_{b,f} \tag{14}$$

where $\underline{\left|\frac{\partial T_{b,f}}{\partial q_h}\right|}^{-1}\underline{\left|\frac{\partial T_{b,f}}{\partial q_h}\right|} = \underline{I}$, the identity matrix. (i.e.,$\underline{\left|\frac{\partial T_{b,f}}{\partial q_h}\right|}^{-1}$ is the inverse matrix).

Differentiating (4):

$$\frac{\partial T_{b,f}}{\partial q_h} = \left[-T_c exp\Big(-\sum_{h'=0}^{\infty}\alpha_{t,h'}\delta h'\Big) + T_h(1-\alpha_{t,h}\delta h)exp\Big(-\sum_{h'=0}^{h}\alpha_{t,h'}\delta h'\Big)\right]\frac{\partial \alpha_{v,h}}{\partial q_h}\delta h \tag{15}$$

To evaluate this derivative, we will need to incorporate a measured temperature profile, and assume a representative first-guess vapor profile. Because we will know the temperature profile (and the surface pressure and therefore the pressure profile) in our inversion method, the partial derivative of α w.r.t. vapor pressure can be written as a total derivative.

We now determine the derivative $\frac{d\alpha_{v,h}}{dq_h}$ for equation (15). The dependence of the Liebe absorption line shape factor upon change in pressure broadening parameter γ is:

$$\frac{\partial F''_v}{\partial \gamma} = f\left[\frac{(f-f_o)^2-\gamma^2}{\big((f-f_o)^2+\gamma^2\big)^2} + \frac{(f+f_o)^2-\gamma^2}{\big((f+f_o)^2+\gamma^2\big)^2}\right] \tag{16}$$

The dependence of γ upon the water vapor partial pressure is:

$$\frac{\partial \gamma}{\partial q_h} = 1.384(b_3 \times 10^{-3})b_4 \tag{17}$$

So,

$$\frac{d\alpha_{v,h}}{dq_h} = \frac{\alpha_{v,h}}{q} + 0.08029 b_1(b_3\times 10^{-3})b_4 q\theta^{2.5}exp\big(b_2(1-\theta)\big)$$
$$\times\frac{f^2}{f_o}\left[\frac{(f-f_o)^2-\gamma^2}{\big((f-f_o)^2+\gamma^2\big)^2} + \frac{(f+f_o)^2-\gamma^2}{\big((f+f_o)^2+\gamma^2\big)^2}\right] + f^2(574\theta^{5.5}q + 6.54\theta^2 p)\times 10^{-10} \tag{18}$$

Summary: The required matrix elements for the clear air case for equation (13) are:

$$\frac{\partial T_{b,f}}{\partial q_h} = \left[-T_c exp\Big(-\sum_{h'=0}^{\infty}\alpha_{t,h'}\delta h'\Big) + T_h(1-\alpha_{t,h}\delta h)exp\Big(-\sum_{h'=0}^{h}\alpha_{t,h'}\delta h'\Big)\right]\frac{d\alpha_{v,h}}{dq_h}\delta h \tag{15}$$

where the absorption due to water vapor is;

$$\alpha_{v,h} = 0.05801 b_1 q \theta^{2.5} exp\big(b_2(1-\theta)\big)\frac{f^2}{f_o}\Big[\frac{\gamma}{(f-f_o)^2+\gamma^2}+\frac{\gamma}{(f+f_o)^2+\gamma^2}\Big]$$

$$+f^2(287\theta^{5.5}q^2 + 6.54\theta^2 pq)\times 10^{-10}\ np/km \tag{11}$$

the total absorption for the clear air case is that of oxygen and water vapor;

$$\alpha_{t,h} \simeq \alpha_{O_2,h} + \alpha_{v,h} \qquad (from\ 6)$$

where the αs are summed over all significant lines and are calculated using the Rosenkranz oxygen model and Liebe's vapor model above;

$$F_v'' = f\Big[\frac{\gamma}{(f-f_o)^2+\gamma^2}+\frac{\gamma}{(f+f_o)^2+\gamma^2}\Big] \tag{7}$$

$$\frac{d\alpha_{v,h}}{dq_h} = \frac{\alpha_{v,h}}{q} + 0.08029 b_1 (b_3\times 10^{-3}) b_4 q\theta^{2.5} exp\big(b_2(1-\theta)\big)$$

$$\times\frac{f^2}{f_o}\left[\frac{(f-f_o)^2-\gamma^2}{\big((f-f_o)^2+\gamma^2\big)^2}+\frac{(f+f_o)^2-\gamma^2}{\big((f+f_o)^2+\gamma^2\big)^2}\right] + f^2(574\theta^{5.5}q + 6.54\theta^2 p)\times 10^{-10} \tag{18}$$

and where:

$$\gamma = (b_3\times 10^{-3})(p\theta^{b_5} + 1.384 b_4 q) \tag{12}$$

Pressures are in millibars, temperatures in Kelvins, frequencies and γ in gigaherz, vapor densities in g/m^3. Because of its small size, one could probably substitute a constant value for the first (cosmic radiation) term on the r.h.s. of (15) above.

References:

Liebe, H.J., 1989; "MPM-An Atmospheric Millimeter-wave Propagation Model," International Journal of Infrared and Millimeter Waves, **10**, No. 6, 1989.

Liebe, H.J., G. A. Hufford, M. G. Cotton, 1993; "Propagation Modeling of Moist Air and Suspended Water/Ice Particles at Frequencies below 1000 GHz," AGARD 52nd Specialists' Meeting of the Electromagnetic Wave Propagation Panel, Palma De Mallorca, Spain, 17-21 May 1993.

Rosenkranz, P.W. 1992; "Atmospheric Remote Sensing by Microwave Radiometry," Chapter 2, M. Janssen, Editor, Wiley, ISBN 0-471-62891-3.

Appendix B

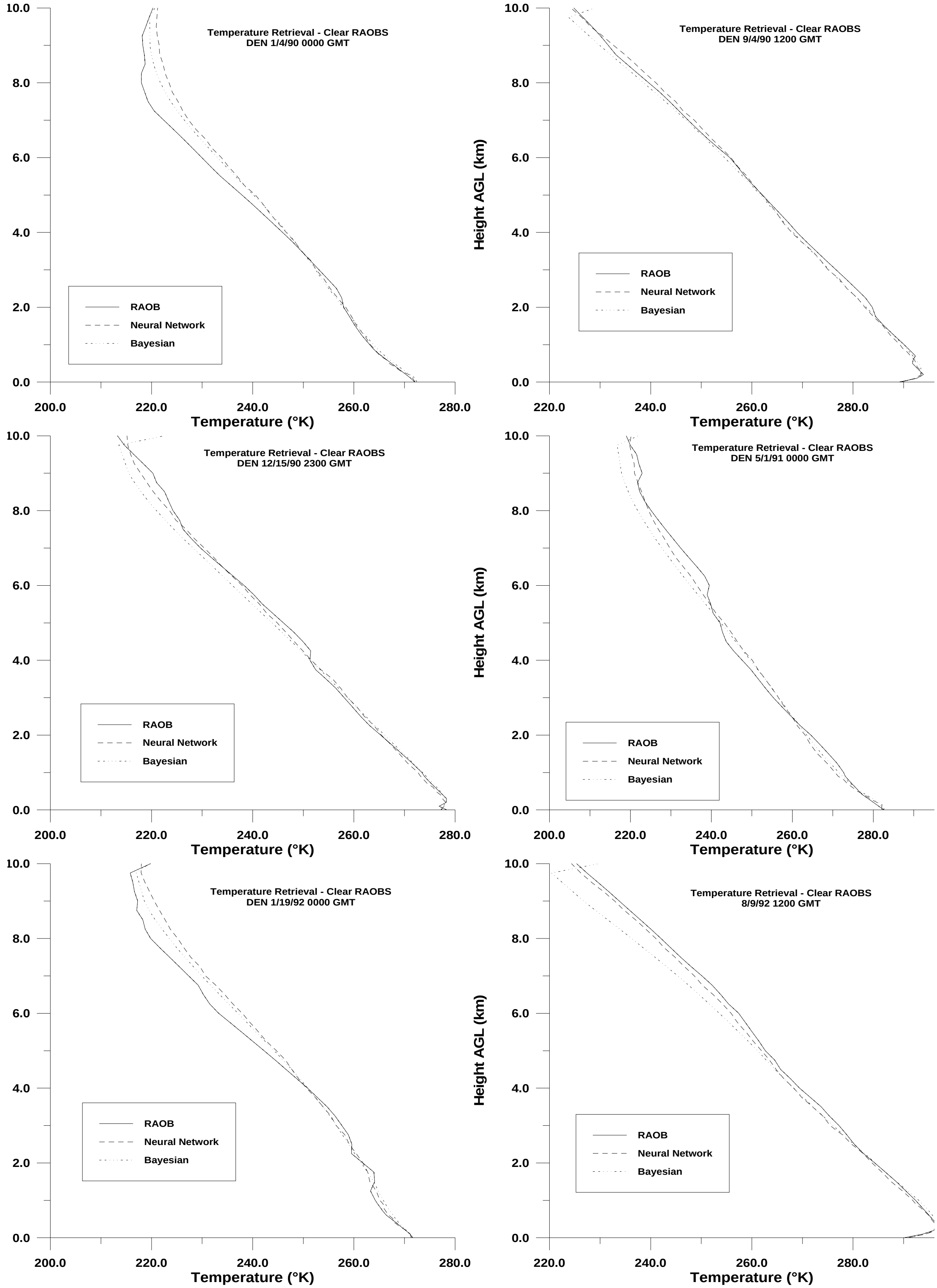

FIGURE 12. Sample neural network temperature profile retrievals for clear conditions at Denver Colorado using all-season retrieval coefficients.

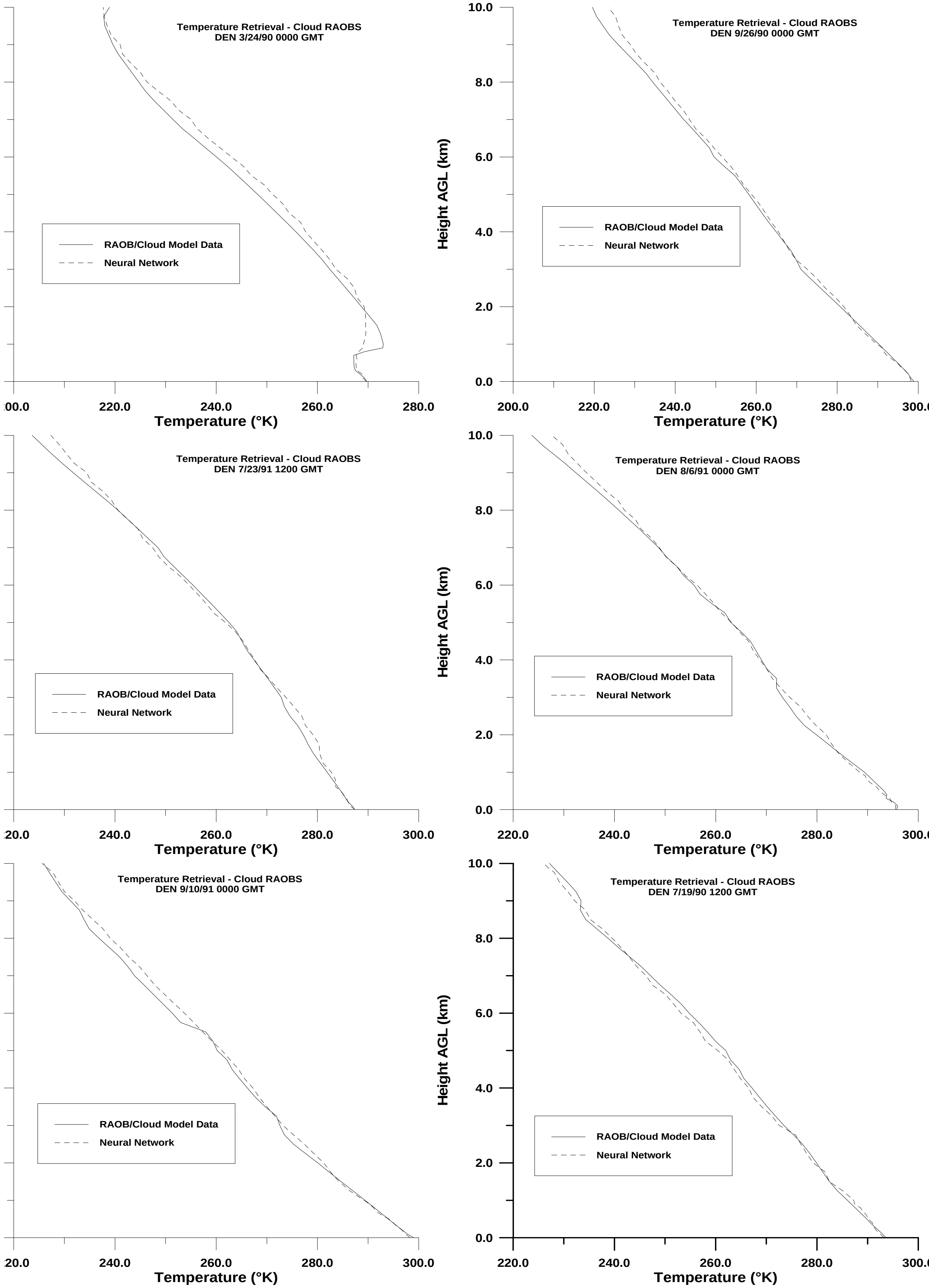

FIGURE 13. Sample neural network temperature profile retrievals for cloudy conditions at Denver Colorado using all-season retrieval coefficients.

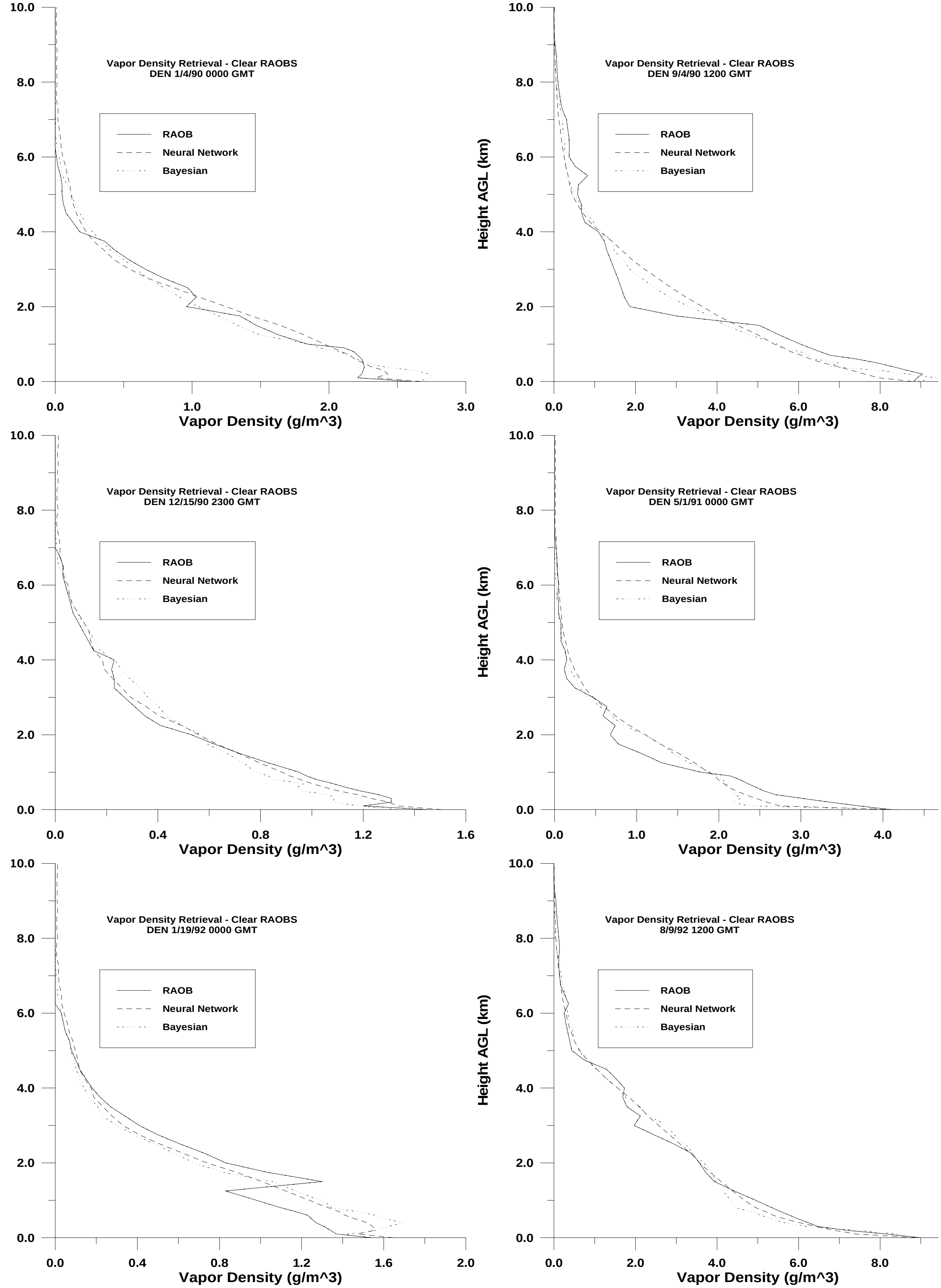

FIGURE 14. Sample Bayesian and neural network water vapor profile retrievals for clear conditions at Denver Colorado using all-season retrieval coefficients.

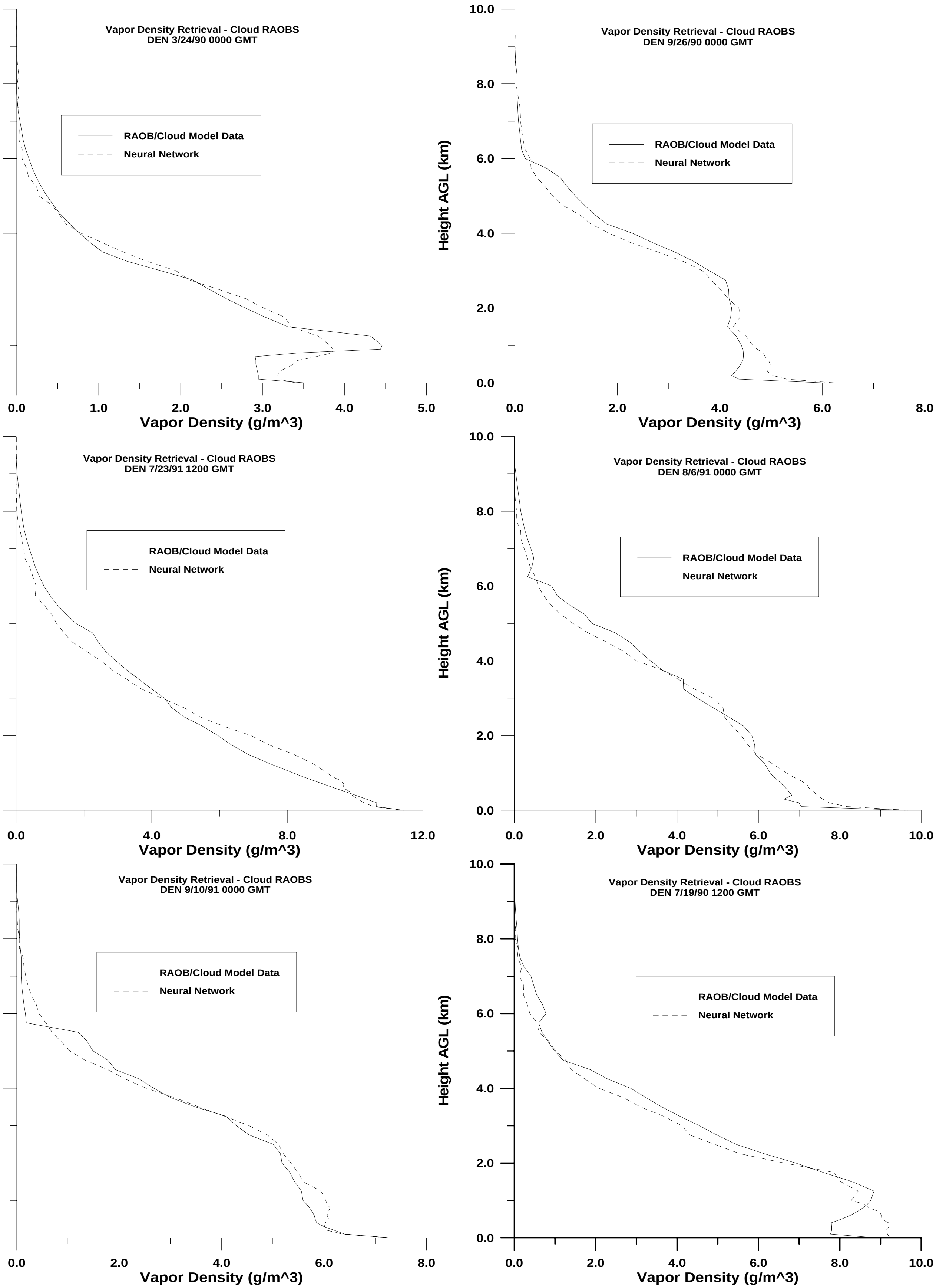

FIGURE 15. Sample neural network water vapor profile retrievals for cloudy conditions at Denver Colorado using all-season retrieval coefficients.

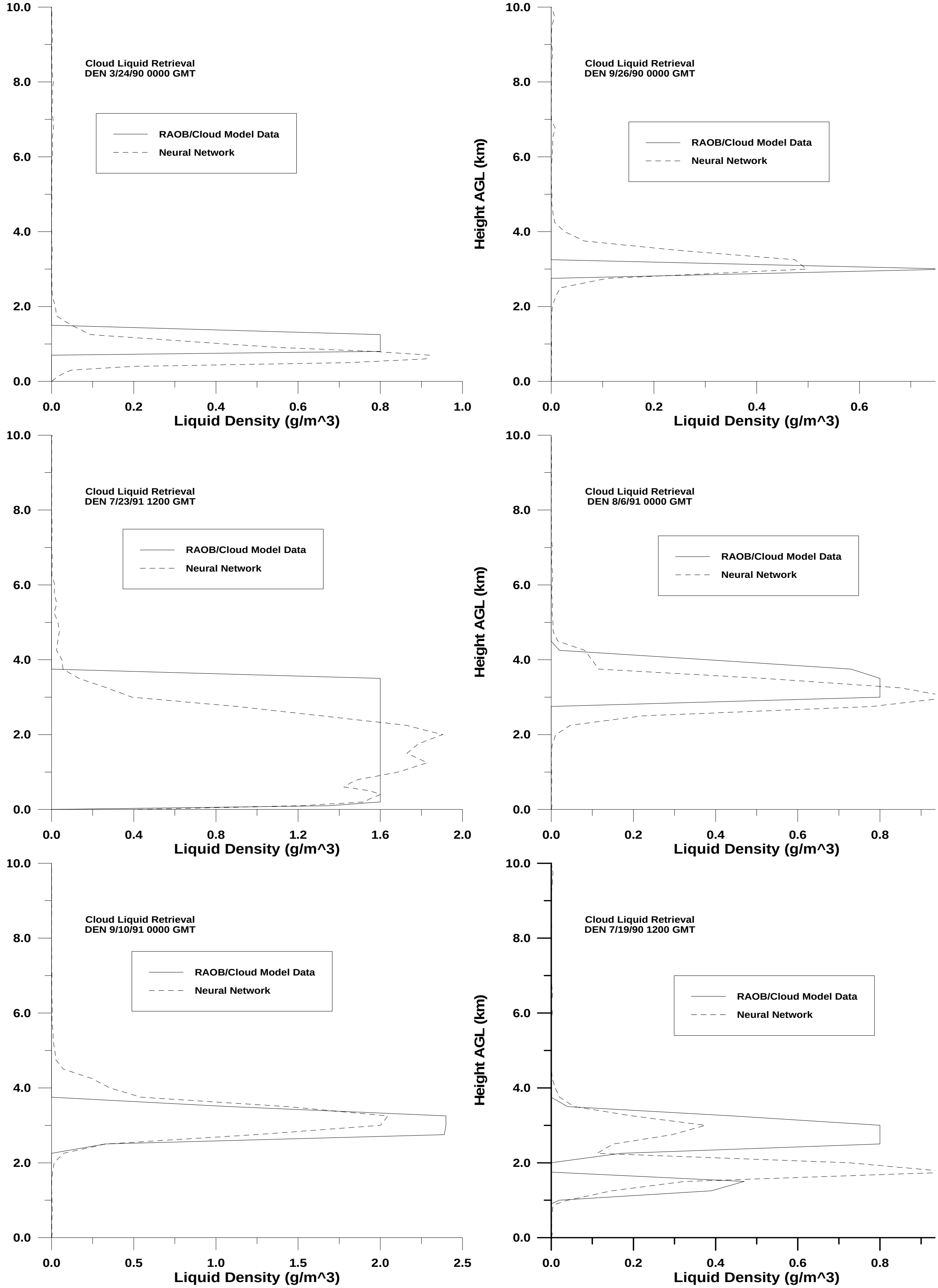

FIGURE 16. Sample neural network cloud liquid water profile retrievals for Denver Colorado using all-season retrieval coefficients.

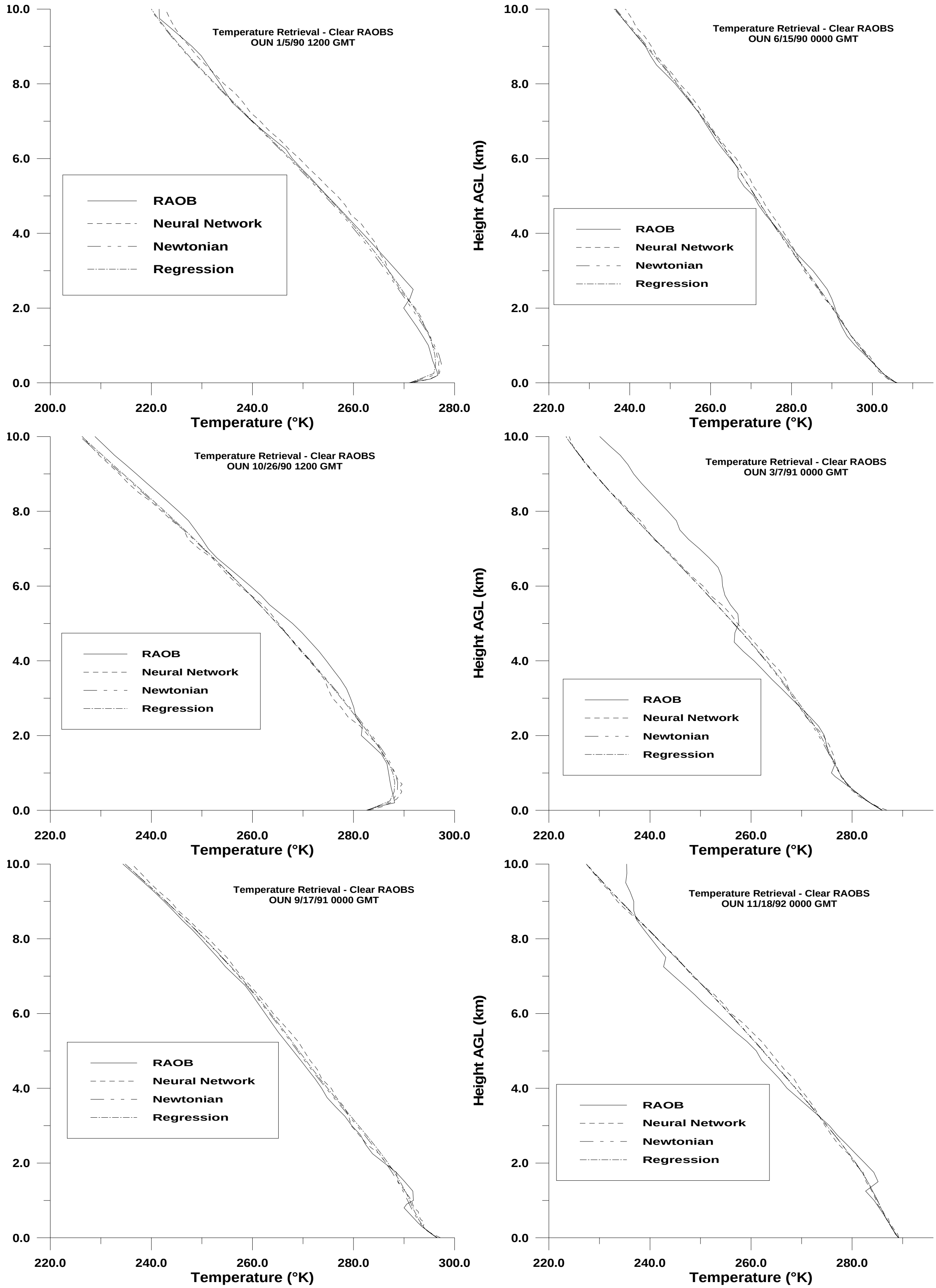

FIGURE 17. Sample neural network, Newtonian iteration, and statistical regression temperature profile retrievals for clear conditions at Norman, Oklahoma using all-season retrieval coefficients.

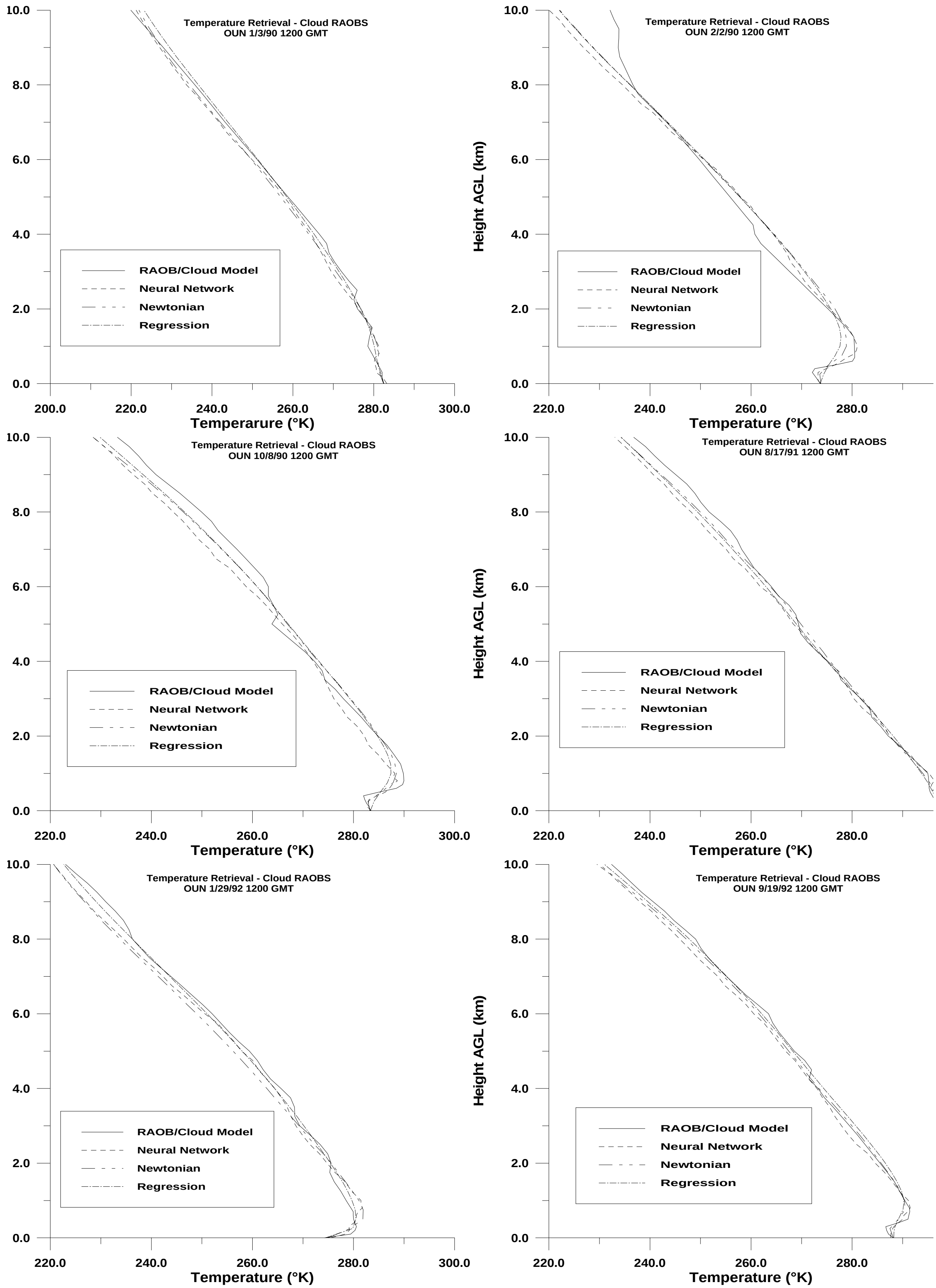

FIGURE 18. Sample neural network, Newtonian iteration, and statistical regression temperature profile retrievals for cloudy condition at Norman, Oklahoma using all-season retrieval coefficients.

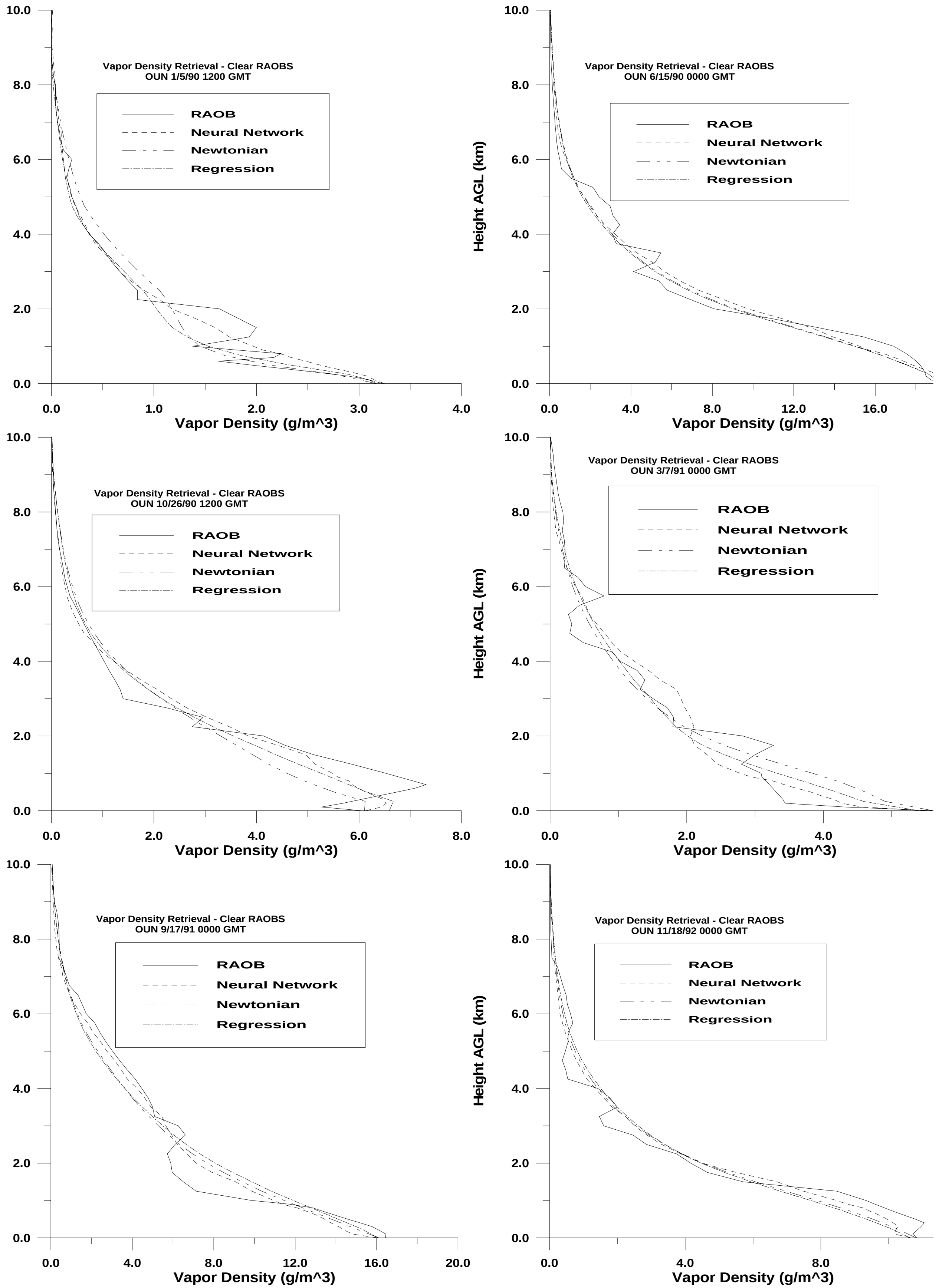

FIGURE 19. Sample neural network, Newtonian iteration, and statistical regression vapor density profile retrievals for clear conditions at Norman, Oklahoma using all-season retrieval coefficients.

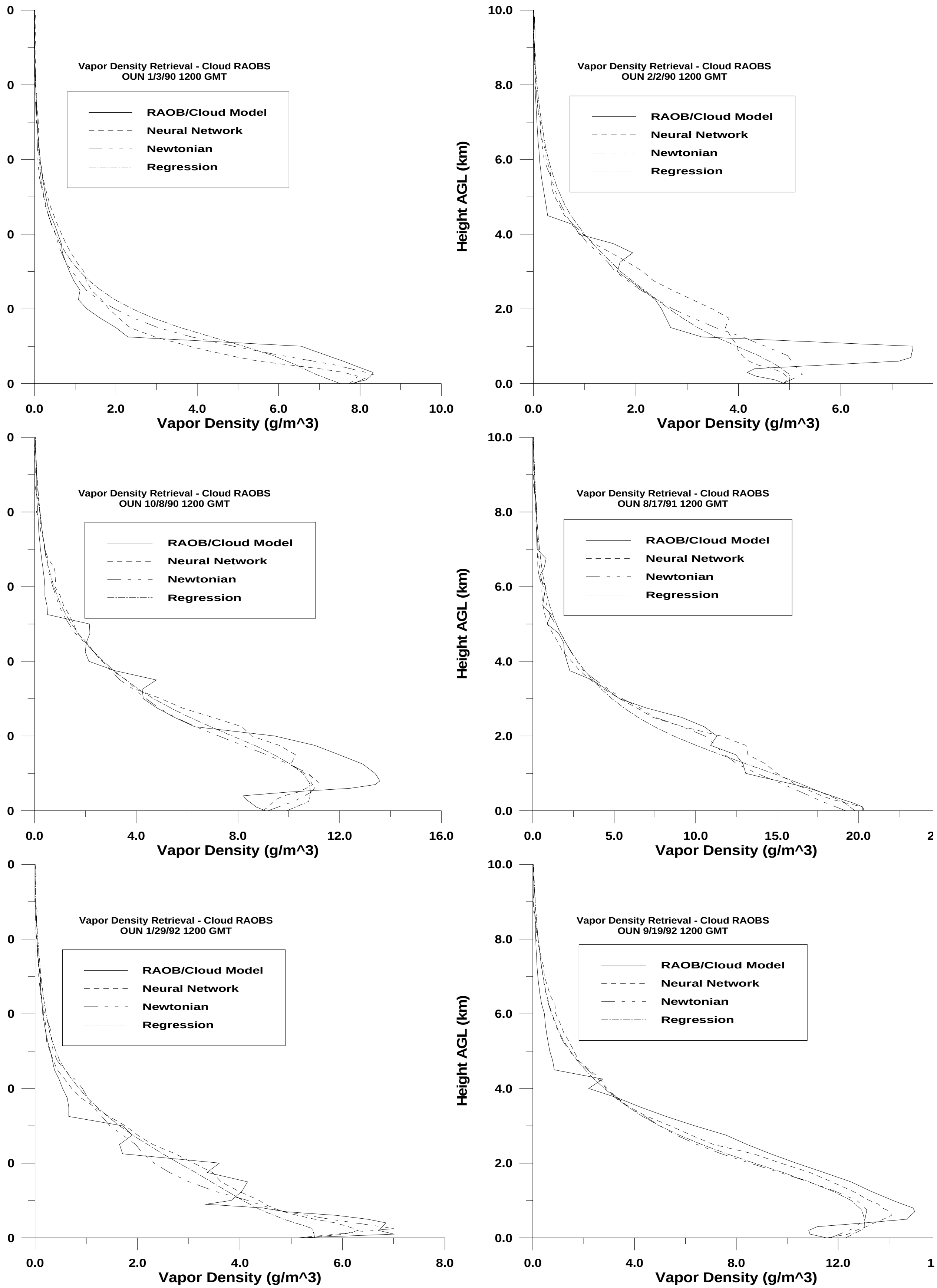

FIGURE 20. Sample neural network, Newtonian iteration, and statistical regression vapor density profile retrievals for cloudy conditions at Norman, Oklahoma using all-season retrieval coefficients.

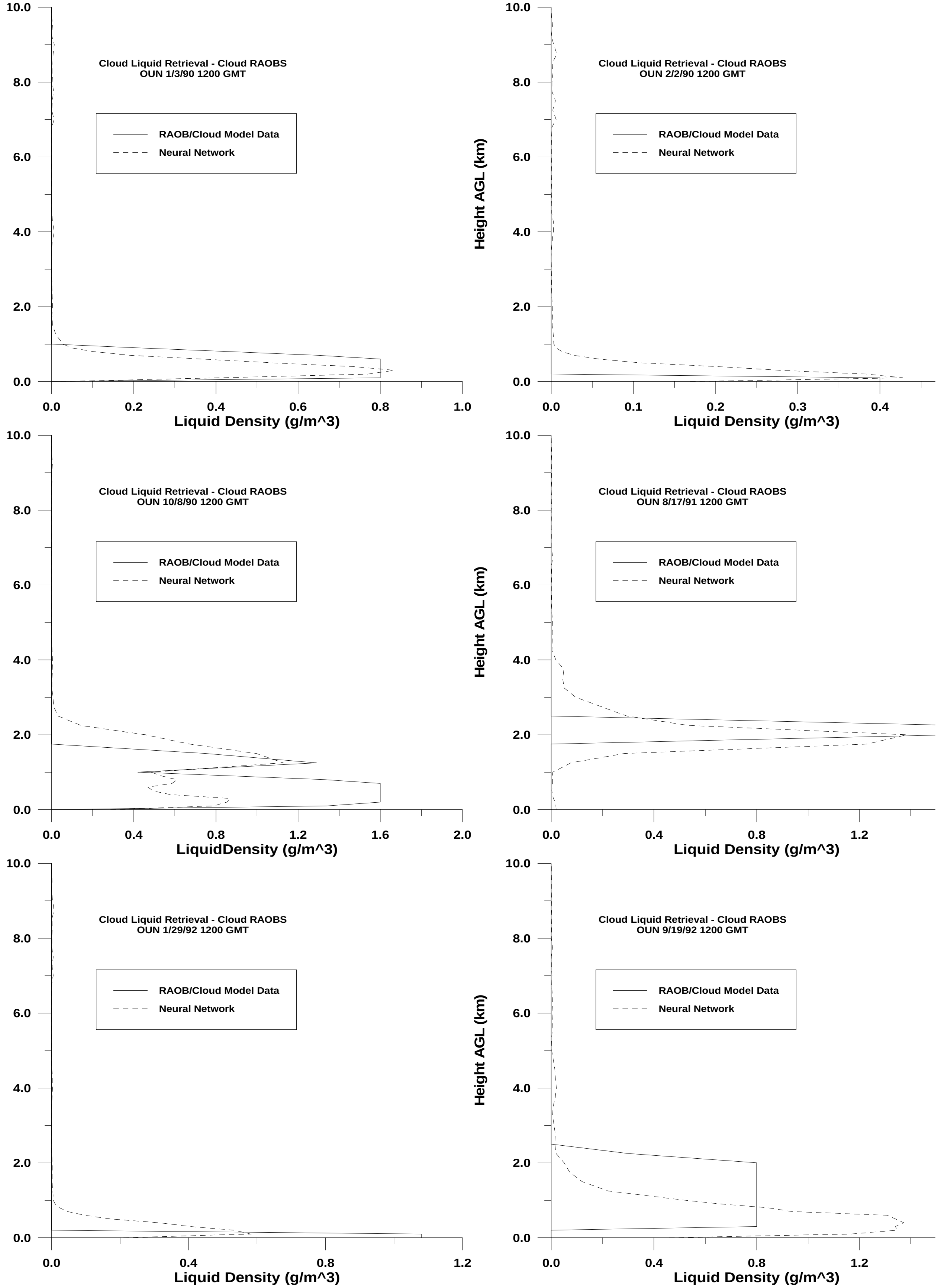

FIGURE 21. Sample neural network cloud liquid profile retrievals at Norman Oklahoma using all-season retrieval coefficients.

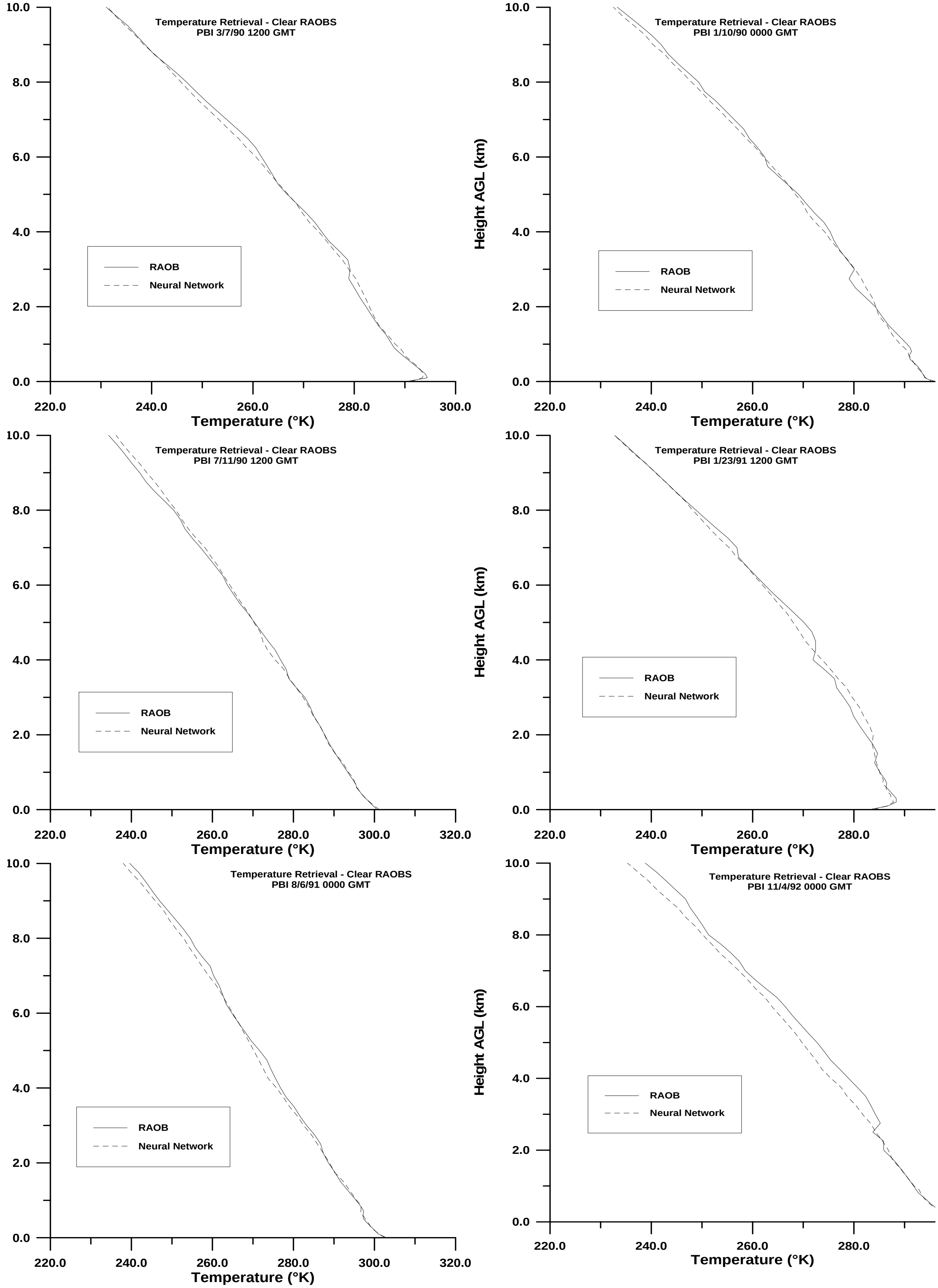

FIGURE 22. Sample neural network temperature profile retrievals for clear conditions at West Palm Beach Florida using all-season retrieval coefficients.

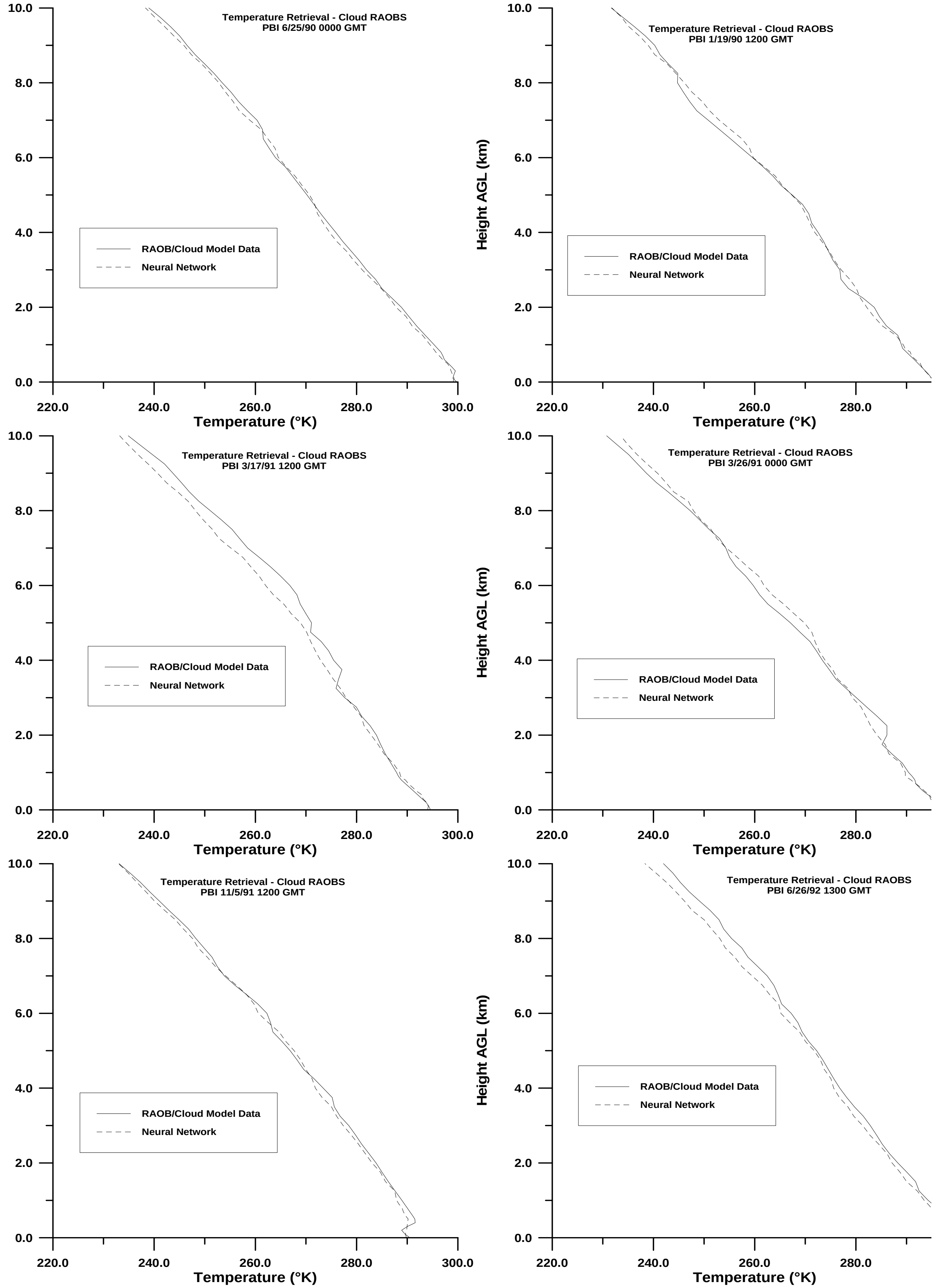

FIGURE 23. Sample neural network temperature profile retrievals for cloudy conditions at West Palm Beach Florida using all-season retrieval coefficients.

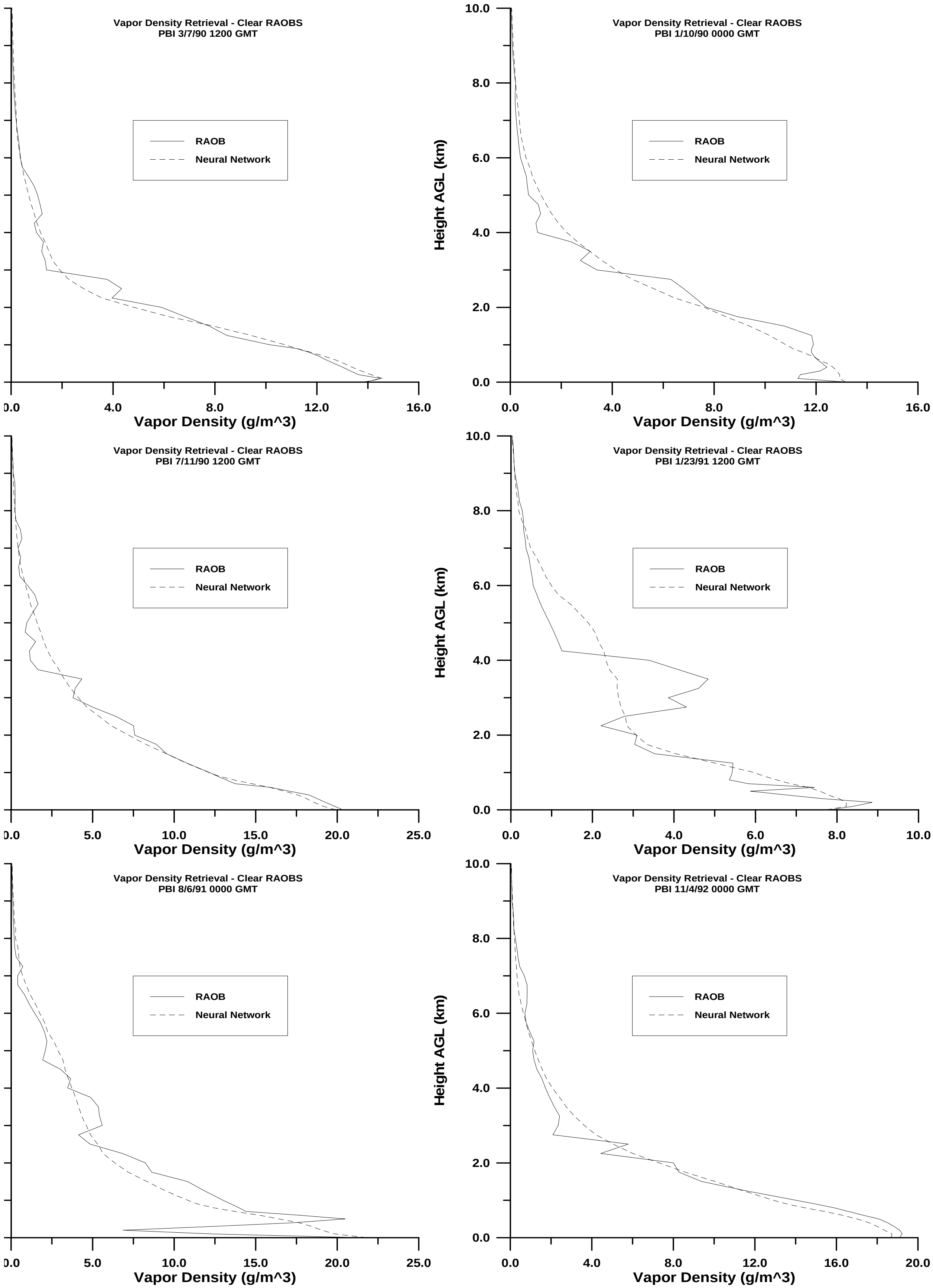

FIGURE 24. Sample neural network water vapor profile retrievals for clear conditions at West Palm Beach Florida using all-season retrieval coefficients.

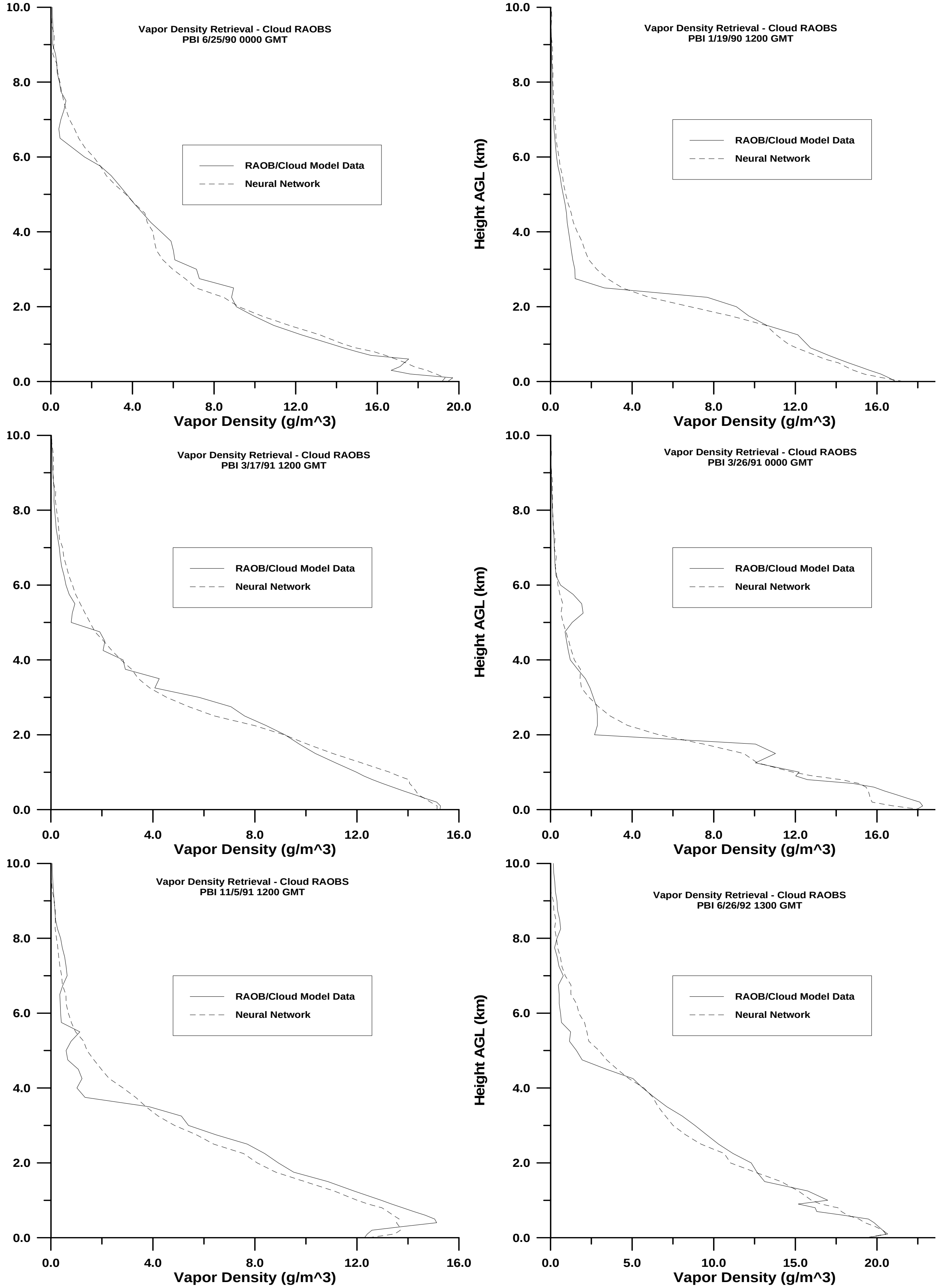

FIGURE 25. Sample neural network water vapor profile retrievals for cloudy conditions at West Palm Beach Florida using all-season retrieval coefficients.

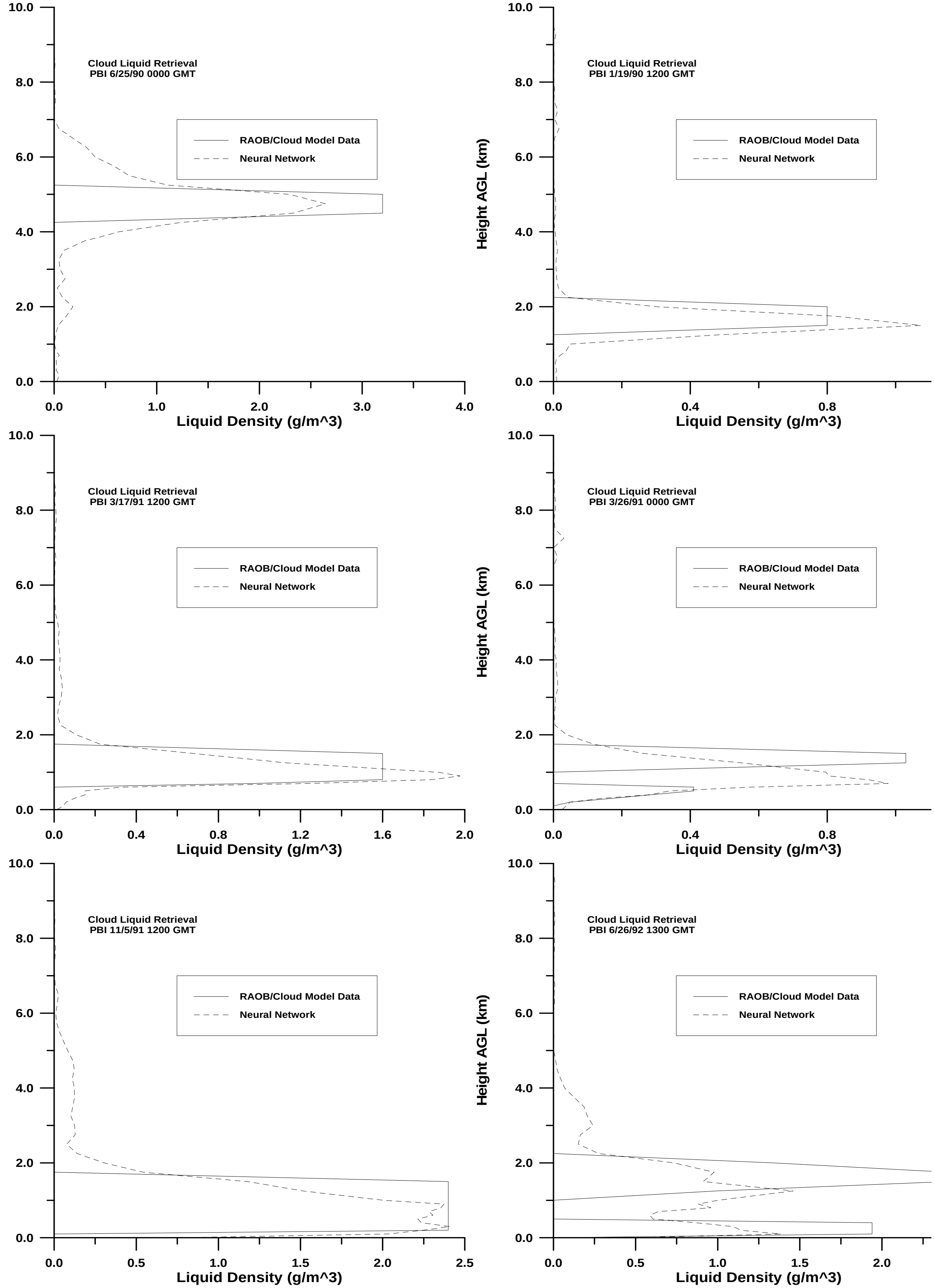

FIGURE 26. Sample neural network cloud liquid water profile retrievals for West Palm Beach Florida using all-season retrieval coefficients.